GUIDED WAVE PROPAGATION IN TUBULAR SECTION WITH MULTI-LAYERED VISCOELASTIC COATING

A Thesis

by

CHI-WEI KUO

Submitted to the Office of Graduate Studies of
Texas A&M University
in partial fulfillment of the requirements for the degree of

MASTER OF SCIENCE

Approved by:

Chair of Committee,	Chii-Der Suh
Committee Members,	Gwo-Ping Fang (Alex)
	Sy-Bor Wen
Head of Department,	Jerald Caton

December 2012

Major Subject: Mechanical Engineering

ABSTRACT

Three kinds of propagating waves physically admissible in a tubular section are derived to establish their dispersion characteristics in response to the presence of multi-layered viscoelastic coatings. One is the longitudinal wave that propagates in the axial direction. The other two are shear and longitudinal waves along the circumferential direction. To characterize the hollow cylinder with coating layers, wave dispersion and attenuation are studied using the "global matrix" technique. Since each layer is considered to be perfectly bonded to each other, displacement and strain continuity are imposed as the interfacial boundary conditions. Viscoelastic coating materials such as bitumen and epoxy serve to improve pipeline reliability, but they also dampen and dissipate wave energy. The viscoelastic materials are studied as well. By replacing the real material constants with complex material constants in the characteristic equation, the impact of the viscoelastic coatings on wave dispersion is established. Bisection method is followed to find the real and complex roots of the three characteristic equations derived. Roots thus obtained are manipulated to allow the phase velocity and attenuation dispersion to be plotted against frequency. The dispersion of phase velocity and wave attenuation for coated pipes are evaluated against a baseline model which is the bare, uncoated tubing to establish the propagation characteristics of the guided shear and longitudinal waves in the presence of multiple coating layers. The effects of increasing attenuation parameter and coating thickness are also investigated.

ACKNOWLEDGEMENTS

I would like to dedicate the thesis to my beloved parents who raised my brother and me with sacrificial love. Their greatness is beyond words. No words of gratitude are worthy of their steadfast love and encouragement.

I would also like to thank my academic advisor, Dr. C Steve Suh, for his support and guidance throughout my study at Texas A&M. His attitude of seriousness toward teaching and research along with his sincerity greatly affected me as a graduate student. My thanks also go to Dr. Fang for serving on my advisory committee and to Dr. Wen for his guidance and support throughout the course of this research.

Finally, I would like to thank all my friends who had helped with great generosity, and colleagues and the department faculty and staff for making my time at Texas A&M University a great experience.

TABLE OF CONTENTS

Page

LIST OF FIGURES

Page

LIST OF TABLES

1. INTRODUCTION

1.1 Overview

Pipelines are found everywhere transporting fluid, gas, water, and all sorts of by-products from one place to another. It is common that pipelines are run either underground or inside a host device where they are not exposed or easily accessible. Pipelines are oftentimes subject to conditions that could compromise their operational reliability. Tubular rupture induced by corrosion, for example, can be both costly and environmentally disastrous. Large scale catastrophic failure to pipelines can also be inflicted by flaws and defects that are of small geometric scale. In general it is preferred that flaws and defects are identified and resolved before they compromise pipeline reliability. Such a preference is what drives the quest for better, cost-effective tubular inspection technologies that are of higher resolution and low false positive.

Defect detection methods of the old days were invasive. They could damage the pipeline, rendering it too costly to justify replacement or repair. Nowadays most pipelines are buried under the surface or submerged subsea, making it even costly to replace if damaged. Non-destructive evaluation is therefore called for. The discovery of ultrasonic evaluation makes it possible to implement NDE technology. The primary benefit of ultrasonic NDE is that the probing ultrasounds are less dissipative than the low frequency waves. Furthermore, it can be used to detect minor defects because the wave length employed is short enough to resolve the small defects. The smaller defect can be

detected, the earlier viable remedial action can be taken to effectively offset the ultimate failure.

Stress wave propagation in finite structures consisting of a single isotropic material has been investigated for decades. Gazis [1] studied harmonic waves propagating in a hollow cylinder. He used the linear theory of elasticity and Helmholtz potential to derive the characteristic equation for the axial symmetric waves and then compared the results to the data generated by the shell theory [2]. Liu and Qu [3] derived the characteristic equation to determine the frequency dispersion curve for the guided circumferential waves in a two-dimensional circular annulus. Valle et al. [4] employed the circumferential guided wave information extracted using Fast Fourier Transform (FFT) to identify the location of a crack along with its length by comparing the results with the model built by the commercial FEA software. Piezoelectric transducers are commonly used to excite ultrasonic guided waves. Hirao and Ogi [5] developed a circumferential SH-wave Electromagnetic Acoustic Transducer (EMAT) technique for the detection of corrosion defects on the outer surface of steel pipelines with or without protective resin coating. However, these transducer-generated waves are of very narrow bandwidth of frequencies, thus having rather limited resolution in making out flaw and defect of different configurations.

Laser induced broadband ultrasonic waves, on the other hand, do not have such a limitation. Gao et al. [6] employed a line-source laser to generate broadband waves to identify an artificially simulated crack along the circumferential direction of a tube. The wave was modeled as a cylindrical shell and the information carried by the waves was

extracted using Fourier Transform. Waves in hollow tubes can be physically acquired using broadband optical technique such as TAP-NDE (thermo-acoustic-photonic non-destructive evaluation) [7]. Propagating waves are generated by a laser pulse in the target tube, and fiber-optical interferometers are used to acquire the wave at a measured distance away from the excitation location. Using time-frequency analysis tools to process the experimental waveform, the information carried by the wave can be extracted. Theoretical model can then be employed to reveal the physical conditions the test tube is in. Through exploring these conditions, the configuration and location of the defect can be established.

There are frequency extracting tools that serve different purposes. Niethammer et al. [8] demonstrated the effectiveness of four different time-frequency analysis tools sufficient for processing dispersive Lamb waves. Liew and Wang [9] were among the first to use wavelet analysis for crack identification in structure. Hem and Melhem [10] used FFT and Continuous Wavelet Transform (CWT) to identify defects in a pre-stressed simply-supported beam. They concluded that CWT was preferred over FFT as the choice feature extraction tool for flaw detection. Gabor wavelet transform was found to provide the resolution needed for resolving fine features indicative of the presence of flaw and defect.

1.2 Literature Review

Pipeline reliability and service life time can be significantly improved using coating materials. Coating materials such as bitumen and epoxy are widely applied to

pipelines for corrosion protection. These materials are viscoelastic and they serve to dampen and dissipate wave energy. For the very reason it is difficult to perform wave generation and acquisition in tubulars with viscoelastic coatings. However, certain types of waves can be initiated in coated pipes and they do not dissipate or attenuate as prominently as others. Therefore, it is considered an important task by many researchers to find the right type of waves to be propagated in coated pipes. While literature on coated or layered pipes is relatively abundant, there are only a handful of studies on wave propagation in viscoelastically coated pipes.

Building a multi-layered tubular model is oftentimes the first step taken to study wave propagation in pipes with viscoelastic coating. Kley et al. [11] studied a two-layered cylindrical component. They used lasers to optically generate circumferential guided waves and then applied FFT to extract the corresponding dispersion curve for comparison with the theoretical results [12]. Jones [13] and Laperre [14] considered the propagation of Lamb waves in bi-layered elastic plates. But they did not explore the effect of internal loss due to viscoelastic damping.

Simonetti [15] studied the attenuation effect of viscoelastic coating on the guided wave in a plate. The internal loss of the guided Lamb wave in response to the coating was modeled using the theory of linear viscoelasticity. The coating material was investigated for its viscoelastic characteristics modeled as a Newtonian viscous fluid by Zhu [16] and by Nayfeh [17]. Luo et al. [18] studied the circumferential guided wave propagation in a viscoelastic multi-layered hollow pipe. Characteristic equations were derived to determine wave dispersion and wave attenuation. They identified the wave

undergoing less energy dissipation and used the finding to develop a protocol for the detection of defects in the coated pipe. Not only were the circumferential guided waves explored. Guided waves along the axial direction have also been studied. Barshinger and Rose [19] studied the longitudinal guided mode in an elastic hollow cylinder with viscoelastic coatings. The characteristic equations for the coated pipe were developed assuming axis-symmetry and by using the global matrix method they were able to study wave dispersion and attenuation imparted by the viscoelastic coating. They also studied the effect of coating thickness on wave characteristics for different coatings.

Little is available on wave propagation in multi-layered coated pipes. In addition, no previous works have considered or modeled perfectly bounded layers using strain continuity boundary conditions between interfacing layers. These two specifics are comprehensively addressed in the thesis.

1.3 Objectives

The primary objective of this study is to explore propagating waves that are physically admissible in a tubular section, so as to establish their dispersion characteristics in response to the presence of multi-layered viscoelastic coatings. The longitudinal guided waves propagating in both the axial and circumferential directions are investigated along with the shear waves that move along the circumferential direction. All the waves are derived from the Navier's equation and their corresponding dispersion curves are established as functions of frequency. It should be mentioned that since each layer is considered to be perfectly bonded to each other, strain continuity is

imposed as the boundary condition. This is in contrast to the stress continuity boundary condition that is followed in some research [19]. The outer and inner surfaces of the tubing are subjected to traction-free forcing conditions. Using these conditions in a hollow cylinder model with two layers of dissimilar viscoelastic coating materials, wave dispersion and the corresponding attenuation effect are established. Results documented in the later part of the thesis are expected to be of practical usefulness to those who practice NDE for pipeline inspection. The roots of the characteristic equation to be derived in the sections that follow are numerically determined using the bisection method.

2. WAVE DISPERSION IN LAYERED HOLLOW CYLINDER

Guided waves initiated in coated pipes are both dispersive and attentuative. Considered characteristically fundamental, dispersion and attenuation are commonly explored to characterize the pipe in which a guided wave propagates for mechanical flaws. Thus it is essential that these wave characteristics are understood at the fundamental level. In the current section several characteristics equations, each corresponds to a particular mode of wave propagation, are derived for a layered, hollow cylinder following the global matrix approach by Knopoff [20] and the notations by Lowe [21]. A general strategy is followed to formulate the characteristics equations. First the governing equation of the propagation mode of interest is derived for a pipe of a single elastic layer. The associated stress, strain, and displacement equations are then developed, followed by applying boundary and interfacial continuity conditions. By expressing these equations in matrices, the system of the multi-layer tubular is represented by assembling the matrices into a "global matrix." The corresponding characteristic equation is then emerged through solving the determinant of the global matrix.

The longitudinal wave propagating along the axial direction in an elastic hollow cylinder is first developed. Since stress waves propagate in both the axial and circumferential directions, it is necessary to also establish the dispersion and attenuation characteristics for the modes that propagate along the circumferential direction. Two circumferential modes, namely longitudinal and shear, are studied. By replacing the

material elastic constants with the complex viscoelastic constants for the layers above the base cylindrical section, the various characteristics of the three types of guided wave modes in the multi-layered tubular can be established.

Fig. 2.1 gives the configuration of a pipe section, while Fig. 2.2 shows the multi-layered cross-section of the pipe. The layer between radii r_1 and r_2 is elastic. The outer layer between radii r_2 and r_3 is the viscoelastic coating material. The axial direction of the cylinder is along the z-axis. The circumferential direction is defined by the θ-axis.

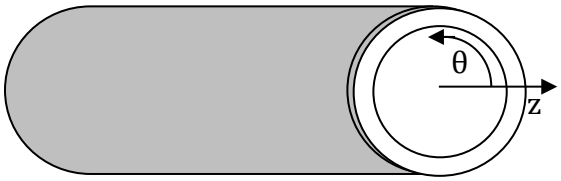

Fig. 2.1 Pipe model

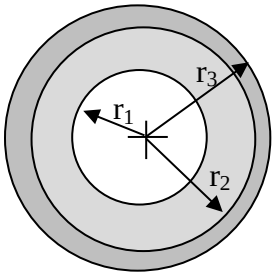

Fig. 2.2 Pipe cross-section

2.1. Longitudinal Wave along Axial Direction

The Lame-Navier equation of motion for isotropic materials is

$$\mu\nabla^2\mathbf{u} + (\lambda + \mu)\nabla(\nabla \cdot \mathbf{u}) = \rho(\partial^2\mathbf{u} / \partial^2 t) \tag{2.1}$$

The Helmholtz theorem dictates that the gradient of a scalar potential function, ϕ, and the curl of a vector potential function, $\mathbf{\Psi}$, can be combined to define the displacement field, $\mathbf{u}$, as

$$\mathbf{u} = \nabla\phi + \nabla \times \mathbf{\Psi} \tag{2.2}$$

with $\nabla \cdot \mathbf{\Psi} = 0$ being an additional constraint. Substituting Eq. (2.2) into Eq. (2.1), one has

$$\mu\nabla^2\left(\nabla\phi + \nabla \times \mathbf{\Psi}\right) + (\lambda + \mu)\nabla(\nabla \cdot \left(\nabla\phi + \nabla \times \mathbf{\Psi}\right)) = \rho(\partial^2\left(\nabla\phi + \nabla \times \mathbf{\Psi}\right)/\partial^2 t) \tag{2.3}$$

Eq. (2.3) can be further simplified by uncoupling the scalar term from the vector function

$$\nabla^2\phi = \frac{\rho}{\lambda + 2\mu}(\partial^2\phi/\partial^2 t) \tag{2.4}$$

$$\nabla^2\mathbf{\Psi} = \frac{\rho}{\mu}(\partial^2\mathbf{\Psi}/\partial^2 t) \tag{2.5}$$

Using Eqs. (2.4) and (2.5), the longitudinal wave velocity c_1 and the shear wave velocity c_2 can be defined as follows

$$c_1 = \sqrt{\frac{\lambda + 2\mu}{\rho}} \tag{2.6}$$

$$c_2 = \sqrt{\frac{\mu}{\rho}} \tag{2.7}$$

Eq. (2.4) and Eq. (2.5) can then be rewritten to represent, respectively, the longitudinal and shear wave equations

$$\nabla^2\phi = \frac{1}{c_1}(\partial^2\phi/\partial^2 t) \tag{2.8}$$

$$\nabla^2 \mathbf{\Psi} = \frac{1}{c_2}(\partial^2 \mathbf{\Psi} / \partial^2 t) \tag{2.9}$$

In the cylindrical coordinate system, the vector potential $\mathbf{\Psi}$ can be defined as the combination of the scalar components $(\psi_r, \psi_\theta, \psi_z)$ and the unit base vector $(\vec{r},\ \vec{\theta},\ \vec{z})$,

$$\mathbf{\Psi} = \psi_r\ \vec{r} + \psi_\theta\ \vec{\theta} + \psi_z\ \vec{z} \tag{2.10}$$

The corresponding Laplacian of the vector potential $\mathbf{\Psi}$ is

$$\nabla^2 \mathbf{\Psi} = \left[\nabla^2 \psi_r - \frac{\psi_r}{r^2} - \frac{2}{r^2}\frac{\partial \psi_\theta}{\partial \theta}\right]\vec{r} + \left[\nabla^2 \psi_\theta - \frac{\psi_\theta}{r^2} + \frac{2}{r^2}\frac{\partial \psi_r}{\partial \theta}\right]\vec{\theta} + \nabla^2 \psi_z \vec{z} \tag{2.11}$$

When the symmetrical wave running along the axial direction is considered, all terms associated with θ are dropped and ψ_r and ψ_z are set to be zero. Additionally, the remaining components ϕ and ψ_θ must only be functions of r and z. Eq. (2.9) is now of the following form as a result.

$$\nabla^2 \psi_\theta - \frac{\psi_\theta}{r^2} = \frac{1}{c_2{}^2}\left(\partial^2 \psi_\theta / \partial^2 t\right) \tag{2.12}$$

Assuming a harmonic wave that propagates in the axial, z-direction, the solutions for the two scalar waves defined in Eqs. (2.8) and (2.12) can be

$$\phi = g(r)e^{i(kz-\omega t)} \tag{2.13}$$

$$\psi_\theta = h(r)e^{i(kz-\omega t)} \tag{2.14}$$

Substituting Eq. (2.13) into Eq. (2.8) and rearranging, Eq. (2.15) results

$$r^2 g''(r) + r g'(r) + r^2 \alpha^2 g(r) = 0 \tag{2.15}$$

with

$$\alpha^2 = \frac{\omega^2}{c_1^{\,2}} - k^2 \tag{2.16}$$

Similarly, substituting Eq. (2.14) into Eq. (2.12), the differential equation becomes

$$r^2 h''(r) + r h'(r) + \left(r^2\beta^2 - 1\right) h(r) = 0 \tag{2.17}$$

with

$$\beta^2 = \frac{\omega^2}{c_2^{\,2}} - k^2 \tag{2.18}$$

Using the zeroth-order type 1 and zeroth-order type 2 Hankel functions defined by the Bessel functions of the first kind and second kind

$$H_n^{1,2}(z) = J_n(z) \pm i Y_n(z) \tag{2.19}$$

the solution for Eq. (2.15) can be expressed as

$$g(r) = A_1 H_0^1(\alpha r) + A_2 H_0^2(\alpha r) \tag{2.20}$$

Similarly the solution for Eq. (2.17) can be expressed using Hankel functions of the first order type 1 and the first order type 2 as

$$h(r) = B_1 H_1^1(\beta r) + B_2 H_1^2(\beta r) \tag{2.21}$$

Substituting Eqs. (2.20) and (2.21) into Eqs. (2.13) and (2.14), the scalar potential ϕ and vector potential component ψ_θ are now

$$\phi = \left[A_1 H_0^1(\alpha r) + A_2 H_0^2(\alpha r)\right] e^{i(kz-\omega t)} \tag{2.22}$$

$$\psi_\theta = \left[B_1 H_1^1(\beta r) + B_2 H_1^2(\beta r)\right] e^{i(kz-\omega t)} \tag{2.23}$$

The divergence of the scalar potential and the curl of the vector potential are

$$\nabla\phi = \frac{\partial\phi}{\partial r}\vec{r} + \frac{1}{r}\frac{\partial\phi}{\partial\theta}\vec{\theta} + \frac{\partial\phi}{\partial z}\vec{z} \tag{2.24}$$

$$\nabla\times\mathbf{\Psi} = \left(\frac{1}{r}\frac{\partial\psi_z}{\partial\theta} - \frac{\partial\psi_\theta}{\partial z}\right)\vec{r} + \left(\frac{\partial\psi_r}{\partial z} - \frac{\partial\psi_z}{\partial r}\right)\vec{\theta} + \frac{1}{r}\left[\frac{\partial}{\partial r}\left(r\psi_\theta\right) - \frac{\partial\psi_r}{\partial\theta}\right]\vec{z} \tag{2.25}$$

With the scalar and vector potential functions properly defined, the components of the displacement vector $\mathbf{u}$ can be formulated as

$$\begin{cases} u_r = \dfrac{\partial\phi}{\partial r} - \dfrac{\partial\psi_\theta}{\partial z} = \left(g' - ikh\right)e^{i(kz-\omega t)} \\ u_\theta = 0 \\ u_z = \dfrac{\partial\phi}{\partial z} + \dfrac{1}{r}\dfrac{\partial}{\partial r}\left(r\psi_\theta\right) = \left(ikg + \dfrac{1}{r}h + h'\right)e^{i(kz-\omega t)} \end{cases} \tag{2.26}$$

Substituting Eqs. (2.20) and (2.21) into Eq. (2.26), the non-zero displacement components take up the following forms with unknown coefficients A_1, A_2, B_1, and B_2

$$u_r = e^{i(kz-\omega t)}\cdot\begin{cases} -\alpha H_1^1\left(\alpha r\right)A_1 \\ -\alpha H_1^2\left(\alpha r\right)A_2 \\ -ikH_1^1\left(\beta r\right)B_1 \\ -ikH_1^2\left(\beta r\right)B_2 \end{cases} \tag{2.27}$$

$$u_z = e^{i(kz-\omega t)}\cdot\begin{cases} ikH_0^1\left(\alpha r\right)A_1 \\ ikH_0^2\left(\alpha r\right)A_2 \\ \beta H_0^1\left(\beta r\right)\beta_1 \\ \beta H_0^2\left(\beta r\right)\beta_2 \end{cases} \tag{2.28}$$

Using the strain-displacement relation, the strains in the cylindrical coordinates are

$$\varepsilon_{rr} = \frac{\partial u_r}{\partial r} = \left(\frac{1}{r}g' - \frac{ik}{r}h\right)e^{i(kz-\omega t)} \tag{2.29}$$

$$\varepsilon_{\theta\theta} = \frac{1}{r}\frac{\partial u_\theta}{\partial \theta} + \frac{u_r}{r} = \left(g'' - ikh'\right)e^{i(kz-\omega t)} \tag{2.30}$$

$$\varepsilon_{rz} = \frac{1}{2}\left(\frac{\partial u_z}{\partial r} + \frac{\partial u_r}{\partial z}\right) = \frac{1}{2}\left(2ikg' + h'' + \frac{1}{r}h' + \left(k^2 - \frac{1}{r^2}\right)h\right)e^{i(kz-\omega t)} \tag{2.31}$$

Substituting Eqs. (2.20) and (2.21) into Eqs. (2.29) and (2.31), the following strain components emerged as a result

$$\varepsilon_{rr} = e^{i(kz-\omega t)} \cdot \begin{cases} \left(-\alpha^2 H_0^1(\alpha r) + \frac{\alpha}{r}H_1^1(\alpha r)\right)A_1 \\ \left(-\alpha^2 H_0^2(\alpha r) + \frac{\alpha}{r}H_1^2(\alpha r)\right)A_2 \\ \left(-ik\beta H_0^1(\beta r) + i\frac{k}{r}H_1^1(\beta r)\right)B_1 \\ \left(-ik\beta H_0^2(\beta r) + i\frac{k}{r}H_1^2(\beta r)\right)B_2 \end{cases} \tag{2.32}$$

$$\varepsilon_{rz} = e^{i(kz-\omega t)} \cdot \begin{cases} -i\alpha k H_1^1(\alpha r)A_1 \\ -i\alpha k H_1^2(\alpha r)A_2 \\ \frac{1}{2}\left(k^2 - \beta^2\right)H_1^1(\beta r)\beta_1 \\ \frac{1}{2}\left(k^2 - \beta^2\right)H_1^2(\beta r)\beta_2 \end{cases} \tag{2.33}$$

By substituting Eqs. (2.29), (2.30), and (2.31) into the Hooke's law below

$$\sigma_{ij} = \lambda\varepsilon_{kk}\delta_{ij} + 2\mu\varepsilon_{ij} \tag{2.34}$$

and invoking

$$\varepsilon_{kk} = \varepsilon_{rr} + \varepsilon_{\theta\theta} + \varepsilon_{zz} \tag{2.35}$$

we have

$$\varepsilon_{kk} = -\left(\alpha^2 + k^2\right)g(r)e^{i(kz-\omega t)} \tag{2.36}$$

Finally, using Eqs. (2.32), (2.33) and (2.36), stress components σ_{rr} and σ_{rz} can be shown to be

$$\sigma_{rr} = e^{i(kz-\omega t)} \cdot \begin{Bmatrix} \left(-\mu\left(\beta^2 - k^2\right) H_0^1\left(\alpha r\right) + \dfrac{2\mu\alpha}{r} H_1^1\left(\alpha r\right)\right) \cdot A_1 \\ \left(-\mu\left(\beta^2 - k^2\right) H_0^2\left(\alpha r\right) + \dfrac{2\mu\alpha}{r} H_1^2\left(\alpha r\right)\right) \cdot A_2 \\ 2\mu\left(-ik\beta H_0^1\left(\beta r\right) + i\dfrac{k}{r} H_1^1\left(\beta r\right)\right) \cdot B_1 \\ 2\mu\left(-ik\beta H_0^2\left(\beta r\right) + i\dfrac{k}{r} H_1^2\left(\beta r\right)\right) \cdot B_2 \end{Bmatrix} \tag{2.37}$$

$$\sigma_{rz} = e^{i(kz-\omega t)} \cdot \begin{Bmatrix} -2i\mu\alpha k H_1^1\left(\alpha r\right) \cdot A_1 \\ -2i\mu\alpha k H_1^2\left(\alpha r\right) \cdot A_2 \\ \mu\left(k^2 - \beta^2\right) H_1^1\left(\beta r\right) \cdot \beta_1 \\ \mu\left(k^2 - \beta^2\right) H_1^2\left(\beta r\right) \cdot \beta_2 \end{Bmatrix} \tag{2.38}$$

Next, boundary conditions are applied to construct the global matrix. For the present problem the exposed inner and outer layers are both traction-free. Interfacial continuity condition requires that the strains and displacements along the two interfacial layers to be continuous for a perfect bond. The stress-free surface boundary conditions are therefore

$$\begin{Bmatrix} \sigma_{rr} \\ \sigma_{rz} \end{Bmatrix}_{surface} = 0 \tag{2.39}$$

The stress components for a single layer are

$$\begin{Bmatrix} \sigma_{rr} \\ \sigma_{rz} \end{Bmatrix} = [D_1] \begin{Bmatrix} A_1 \\ A_2 \\ B_1 \\ B_2 \end{Bmatrix} \tag{2.40}$$

And the corresponding interfacial boundary condition is

$$\begin{Bmatrix} u_r \\ u_z \\ \varepsilon_{rr} \\ \varepsilon_{rz} \end{Bmatrix}_{\substack{layer\ p \\ Interface\ p+1}} = \begin{Bmatrix} u_r \\ u_z \\ \varepsilon_{rr} \\ \varepsilon_{rz} \end{Bmatrix}_{\substack{layer\ p+1 \\ Interface\ p+1}} \tag{2.41}$$

thus defining the continuity of the displacement and strain fields at the interface. The corresponding vector form for a single layer is therefore

$$\begin{Bmatrix} u_r \\ u_z \\ \varepsilon_{rr} \\ \varepsilon_{rz} \end{Bmatrix} = [D_2] \begin{Bmatrix} A_1 \\ A_2 \\ B_1 \\ B_2 \end{Bmatrix} \tag{2.42}$$

The layer matrix $[D_1]$ can be defined as Eq. (2.43); the layer matrix $[D_2]$ can be defined separately by inner layer matrix $[D_{2,i}]$ and outer layer matrix $[D_{2,o}]$ which are shown in Eqs. (2.44) and (2.45). Note that the subscript "i" denotes the inner position of each layer while the subscript "o" denotes the outer position of each layer.

$$[D_1]=\begin{bmatrix} -\mu\left(\beta^2-k^2\right)\cdot H_0^1(\alpha r)+\dfrac{2\mu\alpha}{r}H_1^1(\alpha r) & -\mu\left(\beta^2-k^2\right)\cdot H_0^2(\alpha r)+\dfrac{2\mu\alpha}{r}H_1^2(\alpha r) & 2\mu i\left(-k\beta H_0^1(\beta r)+\dfrac{k}{r}H_1^1(\beta r)\right) & 2\mu i\left(-k\beta H_0^2(\beta r)+\dfrac{k}{r}H_1^2(\beta r)\right) \\ -2i\mu\alpha k H_1^1(\alpha r) & -2i\mu\alpha k H_1^2(\alpha r) & \mu\left(k^2-\beta^2\right)H_1^1(\beta r) & \mu\left(k^2-\beta^2\right)H_1^2(\beta r) \end{bmatrix} \quad (2.43)$$

$$\left[D_{2,i}\right]=\begin{bmatrix} -\alpha H_1^1(\alpha r_i) & -\alpha H_1^2(\alpha r_i) & -ikH_1^1(\beta r_i) & -ikH_1^2(\beta r_i) \\ -ikH_0^1(\alpha r_i) & -ikH_0^2(\alpha r_i) & \beta H_0^1(\beta r_i) & \beta H_0^2(\beta r_i) \\ -\alpha^2 H_0^1(\alpha r_i)+\dfrac{\alpha}{r_i}H_1^1(\alpha r_i) & -\alpha^2 H_0^2(\alpha r_i)+\dfrac{\alpha}{r_i}H_1^2(\alpha r_i) & -ik\beta H_0^1(\beta r_i)+i\dfrac{k}{r_i}H_1^1(\beta r_i) & -ik\beta H_0^2(\beta r_i)+i\dfrac{k}{r_i}H_1^2(\beta r_i) \\ -i\alpha k H_1^1(\alpha r_i) & -i\alpha k H_1^2(\alpha r_i) & \dfrac{1}{2}\left(k^2-\beta^2\right)H_1^1(\beta r_i) & \dfrac{1}{2}\left(k^2-\beta^2\right)H_1^2(\beta r_i) \end{bmatrix} \quad (2.44)$$

$$\left[D_{2,o}\right]=\begin{bmatrix} -\alpha H_1^1(\alpha r_o) & -\alpha H_1^2(\alpha r_o) & -ikH_1^1(\beta r_o) & -ikH_1^2(\beta r_o) \\ -ikH_0^1(\alpha r_o) & -ikH_0^2(\alpha r_o) & \beta H_0^1(\beta r_o) & \beta H_0^2(\beta r_o) \\ -\alpha^2 H_0^1(\alpha r_o)+\dfrac{\alpha}{r_o}H_1^1(\alpha r_o) & -\alpha^2 H_0^2(\alpha r_o)+\dfrac{\alpha}{r_o}H_1^2(\alpha r_o) & -ik\beta H_0^1(\beta r_o)+i\dfrac{k}{r_o}H_1^1(\beta r_o) & -ik\beta H_0^2(\beta r_o)+i\dfrac{k}{r_o}H_1^2(\beta r_o) \\ -i\alpha k H_1^1(\alpha r_o) & -i\alpha k H_1^2(\alpha r_o) & \dfrac{1}{2}\left(k^2-\beta^2\right)H_1^1(\beta r_o) & \dfrac{1}{2}\left(k^2-\beta^2\right)H_1^2(\beta r_o) \end{bmatrix} \quad (2.45)$$

Once the layer matrices $[D_1]$, $[D_{2,i}]$, and $[D_{2,o}]$ are developed, the global matrix can be constructed by assembling each matrix. The traction-free boundary conditions mandate the followings,

$$\left[D_1\right]_i \begin{Bmatrix} A_1 \\ A_2 \\ B_1 \\ B_2 \end{Bmatrix} = \begin{Bmatrix} 0 \\ 0 \end{Bmatrix} \tag{2.46}$$

$$\left[D_1\right]_o \begin{Bmatrix} A_1 \\ A_2 \\ B_1 \\ B_2 \end{Bmatrix} = \begin{Bmatrix} 0 \\ 0 \end{Bmatrix} \tag{2.47}$$

with "i" and "o" referring to the inner and outer surfaces, respectively. Furthermore, the boundary conditions for the perfectly bounded interface are,

$$\left[\left[D_{2,o}\right]_{layer=p} \left[-D_{2,i}\right]_{layer=p+1}\right] \begin{Bmatrix} A_{1,p} \\ A_{2,p} \\ B_{1,p} \\ B_{2,p} \\ A_{1,p+1} \\ A_{2,p+1} \\ B_{1,p+1} \\ B_{2,p+1} \end{Bmatrix} = \begin{Bmatrix} 0 \\ 0 \\ 0 \\ 0 \\ 0 \\ 0 \\ 0 \\ 0 \end{Bmatrix} \tag{2.48}$$

Combining Eqs. (2.46)-(2.48), and using a two-layer model as an example, the global matrix equation is then

$$\begin{bmatrix} [D_1]_i & 0 \\ [D_{2,o}]_{layer=1} & [-D_{2,i}]_{layer=2} \\ 0 & [D_1]_o \end{bmatrix} \begin{Bmatrix} A_{1,1} \\ A_{2,1} \\ B_{1,1} \\ B_{2,1} \\ A_{1,2} \\ A_{2,2} \\ B_{1,2} \\ B_{2,2} \end{Bmatrix} = \begin{Bmatrix} \{0\} \\ \{0\} \end{Bmatrix} \tag{2.49}$$

The characteristic dispersion equation for the longitudinal wave running along the axial direction can therefore be determined by finding the non-trivial solutions of Eq. (2.49),

$$\det\left(\begin{vmatrix} [D_1]_i & 0 \\ [D_{2,o}]_{layer=1} & [-D_{2,i}]_{layer=2} \\ 0 & [D_1]_o \end{vmatrix}\right) = 0 \tag{2.50}$$

Using Eq. (2.50), the dispersion of the axial wave can be determined by plotting the phase velocity as a function of the frequency. A numerical scheme is adopted in Sec. 4 to perform this particular task. Using the dispersion equation but replacing the real material constants with complex material constants, the impact of the viscoelasticity of the layer materials can be established. In the followings, the characteristic equation for the shear wave propagating along the circumferential direction is derived.

2.2. Shear Wave along Circumferential Direction

The Lame-Navier equation of motion for isotropic materials that support shear wave propagation is

$$\mu\nabla^2 u_z = \rho\left(\partial^2 u_z / \partial^2 t\right) \tag{2.51}$$

where the corresponding shear velocity is

$$c_2 = \sqrt{\frac{\mu}{\rho}} \tag{2.52}$$

Substituting Eqs. (2.2) and (2.52) into Eq. (2.51), and applying the ∇^2 operator in the cylindrical coordinates, one has

$$\left(\frac{\partial^2 u_z}{\partial r^2} + \frac{1}{r}\frac{\partial u_z}{\partial r} + \frac{1}{r^2}\frac{\partial^2 u_z}{\partial \theta^2}\right) = \frac{1}{c_2^{\,2}}\left(\partial^2 u_z / \partial^2 t\right) \tag{2.53}$$

For a harmonic wave moving in the z-direction, the following solution to Eq. (2.53) can be assumed

$$u_z = h(r)e^{i(kb\theta - \omega t)} \tag{2.54}$$

where *b* is the radius of the entire tubular. Use the solution to expand the wave equation Eq. (2.53) and the following emerges

$$h''(r) + \frac{1}{r}h'(r) + \left[\frac{\omega^2}{c_2^{\,2}} - \left(\frac{kb}{r}\right)^2\right]h(r) = 0 \tag{2.55}$$

whose solution is of the Bessel's type as follows

$$h(r) = A_3 J_{kb}\left(\frac{\omega r}{c_2}\right) + A_4 Y_{kb}\left(\frac{\omega r}{c_2}\right) \tag{2.56}$$

The displacement u_z then becomes

$$u_z = \left[A_3 J_{kb}\left(\frac{\omega r}{c_2}\right) + A_4 Y_{kb}\left(\frac{\omega r}{c_2}\right)\right]e^{i(kb\theta - \omega t)} \tag{2.57}$$

Using the displacement function, all strain components can be obtained as follows by considering the strain-displacement constitutive relationships in the cylindrical coordinate system,

$$\varepsilon_{rr} = \frac{\partial u_r}{\partial r} = 0 \tag{2.58}$$

$$\varepsilon_{\theta\theta} = \frac{1}{r}\frac{\partial u_\theta}{\partial \theta} + \frac{u_r}{r} = 0 \tag{2.59}$$

$$\varepsilon_{zz} = \frac{\partial u_z}{\partial z} = 0 \tag{2.60}$$

$$\varepsilon_{r\theta} = \frac{1}{2}\left(\frac{1}{r}\frac{\partial u_r}{\partial \theta} + \frac{\partial u_\theta}{\partial r} - \frac{u_\theta}{r}\right) = 0 \tag{2.61}$$

$$\varepsilon_{rz} = \frac{1}{2}\left(\frac{\partial u_z}{\partial r} + \frac{\partial u_r}{\partial z}\right) = \frac{1}{2}\frac{\partial u_z}{\partial r} = \frac{1}{2}h'(r)e^{i(kb\theta-\omega t)} \tag{2.62}$$

$$\varepsilon_{\theta z} = \frac{1}{2}\left(\frac{\partial u_\theta}{\partial z} + \frac{1}{r}\frac{\partial u_z}{\partial \theta}\right) = \frac{ikb}{2r}h(r)e^{i(kb\theta-\omega t)} \tag{2.63}$$

The strain component ε_{rz} is obtained by substituting Eq. (2.56) into Eq. (2.62),

$$\varepsilon_{rz} = \frac{\omega}{2C_2}e^{i(kb\theta-\omega t)}\left(\begin{array}{l}\left(J_{kb-1}\left(\frac{\omega r_i}{c_2}\right) - J_{kb+1}\left(\frac{\omega r_i}{c_2}\right)\right)A_3 \\ +\left(Y_{kb-1}\left(\frac{\omega r_i}{c_2}\right) - Y_{kb+1}\left(\frac{\omega r_i}{c_2}\right)\right)A_4\end{array}\right) \tag{2.64}$$

where A_3 and A_4 are coefficients. Applying the Hooke's law, the corresponding stress component is then

$$\sigma_{rz} = \frac{\mu\omega}{c_2} e^{i(kb\theta-\omega t)} \cdot \left\{ \begin{array}{l} \left[J_{kb-1}\left(\frac{\omega r}{c_2}\right) - J_{kb+1}\left(\frac{\omega r}{c_2}\right) \right] \cdot A_3 \\ + \left[Y_{kb-1}\left(\frac{\omega r}{c_2}\right) - Y_{kb+1}\left(\frac{\omega r}{c_2}\right) \right] \cdot A_4 \end{array} \right\} \tag{2.65}$$

Now that the displacement, stress, and strain components are determined, the next is to apply boundary conditions to get the global matrix needed for deriving the dispersion equation. The boundary conditions at traction-free surface is

$$\{\sigma_{rz}\}_{surface} = 0 \tag{2.66}$$

Substitute Eq. (2.65) into Eq. (2.66) and the stress is expressed in the matrix form as

$$\{\sigma_{rz}\} = [D_3] \begin{Bmatrix} A_3 \\ A_4 \end{Bmatrix} \tag{2.67}$$

where

$$[D_3] = \left[J_{kb-1}\left(\frac{\omega r}{c_2}\right) - J_{kb+1}\left(\frac{\omega r}{c_2}\right) \quad Y_{kb-1}\left(\frac{\omega r}{c_2}\right) - Y_{kb+1}\left(\frac{\omega r}{c_2}\right) \right] \tag{2.68}$$

The boundary condition for a perfectly bonded interface is

$$\begin{Bmatrix} u_z \\ \varepsilon_{rz} \end{Bmatrix}_{\substack{layer\ \mathrm{p} \\ \mathrm{Interface\ p+1}}} = \begin{Bmatrix} u_z \\ \varepsilon_{rz} \end{Bmatrix}_{\substack{layer\ \mathrm{p+1} \\ \mathrm{Interface\ p+1}}} \tag{2.69}$$

which again indicates that the displacement and strain fields are continuous. Substitute Eqs. (2.57) and (2.64) into Eq. (2.69), the boundary conditions become

$$\begin{Bmatrix} u_z \\ \varepsilon_{rz} \end{Bmatrix} = [D_4] \begin{Bmatrix} A_3 \\ A_4 \end{Bmatrix} \tag{2.70}$$

The layer matrix $[D_4]$ can be defined separately by the inner layer matrix $[D_{4,\mathrm{i}}]$ and the outer layer matrix $[D_{4,\mathrm{o}}]$ given below, where the subscripts "i" and "o" follow from the same definitions found in Eqs. (2.44) and (2.45) .

$$[D_{4.i}]=\begin{bmatrix} J_{kb}\left(\frac{\omega r_i}{c_2}\right) & Y_{kb}\left(\frac{\omega r_i}{c_2}\right) \\ \frac{\omega}{2C_2}\left(J_{kb-1}\left(\frac{\omega r_i}{c_2}\right)-J_{kb+1}\left(\frac{\omega r_i}{c_2}\right)\right) & \frac{\omega}{2C_2}\left(Y_{kb-1}\left(\frac{\omega r_i}{c_2}\right)-Y_{kb+1}\left(\frac{\omega r_i}{c_2}\right)\right) \end{bmatrix} \tag{2.71}$$

$$[D_{4.o}]=\begin{bmatrix} J_{kb}\left(\frac{\omega r_o}{c_2}\right) & Y_{kb}\left(\frac{\omega r_o}{c_2}\right) \\ \frac{\omega}{2C_2}\left(J_{kb-1}\left(\frac{\omega r_o}{c_2}\right)-J_{kb+1}\left(\frac{\omega r_o}{c_2}\right)\right) & \frac{\omega}{2C_2}\left(Y_{kb-1}\left(\frac{\omega r_o}{c_2}\right)-Y_{kb+1}\left(\frac{\omega r_o}{c_2}\right)\right) \end{bmatrix} \tag{2.72}$$

With the availability of $[D_3]$, $[D_{4,\mathrm{i}}]$, and $[D_{4,\mathrm{o}}]$, the global matrix can be constructed. The boundary conditions for the inner and outer traction-free surfaces are

$$[D_3]_i\begin{Bmatrix} A_3 \\ A_4 \end{Bmatrix}=\begin{Bmatrix} 0 \\ 0 \end{Bmatrix} \tag{2.73}$$

$$[D_3]_o\begin{Bmatrix} A_3 \\ A_4 \end{Bmatrix}=\begin{Bmatrix} 0 \\ 0 \end{Bmatrix} \tag{2.74}$$

Furthermore, along the perfectly bonded interface, the boundary conditions are

$$\left[\left[D_{4,o}\right]_{layer=p}\left[-D_{4,i}\right]_{layer=p+1}\right]\begin{Bmatrix} A_{3,p} \\ A_{4,p} \\ A_{3,p+1} \\ A_{4,p+1} \end{Bmatrix}=\begin{Bmatrix} 0 \\ 0 \\ 0 \\ 0 \end{Bmatrix} \tag{2.75}$$

Applying Eq. (2.73)-(2.75) to a two-layer hollow cylinder model, the global matrix equation becomes

$$\begin{bmatrix} [D_3]_i & 0 \\ [D_{4,o}]_{layer=1} & [-D_{4,i}]_{layer=2} \\ 0 & [D_3]_o \end{bmatrix} \begin{Bmatrix} A_{3,1} \\ A_{4,1} \\ A_{3,2} \\ A_{4,2} \end{Bmatrix} = \begin{Bmatrix} \{0\} \\ \{0\} \end{Bmatrix} \tag{2.76}$$

The corresponding characteristic dispersion equation for the circumferential shear wave can be obtained by setting the following determinant to zero:

$$\det\left(\begin{vmatrix} [D_3]_i & 0 \\ [D_{4,o}]_{layer=1} & [-D_{4,i}]_{layer=2} \\ 0 & [D_3]_o \end{vmatrix} \right) = 0 \tag{2.77}$$

Using Eq. (2.77), the dispersion of the circumferential shear wave can be determined by plotting the phase velocity as a function of the frequency. A numerical scheme is adopted in Sec. 4 to perform this particular task. Using the dispersion equation but replacing the real material constants with complex material constants, the impact of the viscoelasticity of the layer materials can be established. Next, the characteristic equation for the longitudinal wave propagating along the circumferential direction is derived.

2.3. Longitudinal Wave along Circumferential Direction

The Lame-Navier equation of motion for isotropic materials is

$$\mu\nabla^2\mathbf{u} + (\lambda + \mu)\nabla(\nabla \cdot \mathbf{u}) = \rho\left(\partial^2\mathbf{u}/\partial^2 t\right) \tag{2.78}$$

The Helmholtz theorem dictates that the corresponding displacement solution is a function of a scalar potential ϕ and a vector potential $\mathbf{\Psi}$,

$$\mathbf{u} = \nabla\phi + \nabla \times \mathbf{\Psi} \tag{2.79}$$

with $\nabla \cdot \boldsymbol{\Psi} = 0$ as an additional constraint condition. Substituting Eq. (2.79) into Eq. (2.78), the equation of motion becomes

$$\mu \nabla^2 \left(\nabla \phi + \nabla \times \boldsymbol{\Psi} \right) + \left(\lambda + \pi \right) \nabla \left(\nabla \cdot \left(\nabla \phi + \nabla \times \boldsymbol{\Psi} \right) \right) = \rho \left(\partial^2 \left(\nabla \phi + \nabla \times \boldsymbol{\Psi} \right) / \partial^2 t \right) \quad (2.80)$$

The scalar term can be decoupled from the vector term to obtain the followings

$$\nabla^2 \phi = \frac{\rho}{\lambda + 2\mu} (\partial^2 \phi / \partial^2 t) = \frac{1}{c_1} (\partial^2 \phi / \partial^2 t) \quad (2.81)$$

$$\nabla^2 \boldsymbol{\Psi} = \frac{\rho}{\mu} (\partial^2 \boldsymbol{\Psi} / \partial^2 t) = \frac{1}{c_2} (\partial^2 \boldsymbol{\Psi} / \partial^2 t) \quad (2.82)$$

where c_1 and c_2 are longitudinal and shear wave velocities, respectively, as also previously found in Eqs. (2.6) and (2.7).

In the cylindrical coordinate system, the vector potential $\boldsymbol{\Psi}$ can be defined using the scalar components $\left(\psi_r, \psi_\theta, \psi_z \right)$ and unit base vector $\left(\vec{r}, \vec{\theta}, \vec{z} \right)$ as

$$\boldsymbol{\Psi} = \psi_r \vec{r} + \psi_\theta \vec{\theta} + \psi_z \vec{z} \quad (2.83)$$

The Laplacian of $\boldsymbol{\Psi}$ is therefore

$$\nabla^2 \boldsymbol{\Psi} = \left[\nabla^2 \psi_r - \frac{\psi_r}{r^2} - \frac{2}{r^2} \frac{\partial \psi_\theta}{\partial \theta} \right] \vec{r} + \left[\nabla^2 \psi_\theta - \frac{\psi_\theta}{r^2} + \frac{2}{r^2} \frac{\partial \psi_r}{\partial \theta} \right] \vec{\theta} + \nabla^2 \psi_z \vec{z} \quad (2.84)$$

To study the axially symmetric wave behaviors along the circumferential direction, ψ_r and ψ_θ are set to zero as they are functions of the spatial variable z. Additionally, the remaining components ϕ and ψ_z must only be functions of r and θ. Eq. (2.84) now takes up the form

$$\nabla^2 \psi_z = \frac{1}{c_2} (\partial^2 \psi_z / \partial^2 t) \quad (2.85)$$

Since the wave is assumed to be harmonic and propagate along the circumferential θ -direction, the following solutions of Eqs. (2.81) and (2.85) are assumed

$$\phi = g(r)e^{i(kb\theta-\omega t)} \tag{2.86}$$

$$\psi_z = h(r)e^{i(kb\theta-\omega t)} \tag{2.87}$$

where b is the total thickness of the tubular section including the coating layers.

Substituting Eq. (2.86) into Eq. (2.81), the scalar function becomes

$$g''(r)+\frac{1}{r}g'(r)+\left[\frac{\omega^2}{c_1^2}-\left(\frac{kb}{r}\right)^2\right]g(r)=0 \tag{2.88}$$

Similarly, substituting Eq. (2.87) into Eq. (2.85), the vector function becomes

$$h''(r)+\frac{1}{r}h'(r)+\left[\frac{\omega^2}{c_2^2}-\left(\frac{kb}{r}\right)^2\right]h(r)=0 \tag{2.89}$$

It can be shown that $g(r)$ and $h(r)$ are both functions of the Bessel functions

$$g(r)=A_5J_{kb}\left(\frac{\omega r}{c_1}\right)+A_6Y_{kb}\left(\frac{\omega r}{c_1}\right) \tag{2.90}$$

$$h(r)=B_5J_{kb}\left(\frac{\omega r}{c_2}\right)+B_6Y_{kb}\left(\frac{\omega r}{c_2}\right) \tag{2.91}$$

Using Eqs. (2.90) and (2.91), the scalar potential ϕ and the vector potential component ψ_z are now

$$\phi=\left[A_5J_{kb}\left(\frac{\omega r}{c_1}\right)+A_6Y_{kb}\left(\frac{\omega r}{c_1}\right)\right]e^{i(kb\theta-\omega t)} \tag{2.92}$$

$$\psi_z = \left[B_5 J_{kb}\left(\frac{\omega r}{c_2}\right) + B_6 Y_{kb}\left(\frac{\omega r}{c_2}\right)\right] e^{i(kb\theta-\omega t)} \tag{2.93}$$

The divergence of the scalar potential $\nabla\phi$ and the curl of the vector potential $\nabla\times\mathbf{\Psi}$ are utilized

$$\nabla\phi = \frac{\partial\phi}{\partial r}\vec{r} + \frac{1}{r}\frac{\partial\phi}{\partial\theta}\vec{\theta} + \frac{\partial\phi}{\partial z}\vec{z} \tag{2.94}$$

$$\nabla\times\mathbf{\Psi} = \left(\frac{1}{r}\frac{\partial\psi_z}{\partial\theta} - \frac{\partial\psi_\theta}{\partial z}\right)\vec{r} + \left(\frac{\partial\psi_r}{\partial z} - \frac{\partial\psi_z}{\partial r}\right)\vec{\theta} + \frac{1}{r}\left[\frac{\partial}{\partial r}\left(r\psi_\theta\right) - \frac{\partial\psi_r}{\partial\theta}\right]\vec{z} \tag{2.95}$$

to determine the components of the displacement vector $\mathbf{u}$, as follows:

$$u_r = \frac{\partial\phi}{\partial r} + \frac{1}{r}\frac{\partial\psi_z}{\partial\theta} = \left(g' + \frac{ikb}{r}h\right)e^{i(kb\theta-\omega t)} \tag{2.96}$$

$$u_\theta = \frac{1}{r}\frac{\partial\phi}{\partial\theta} - \frac{\partial\psi_z}{\partial r} = \left(\frac{ikb}{r}g - h'\right)e^{i(kb\theta-\omega t)} \tag{2.97}$$

$$u_z = 0 \tag{2.98}$$

Substituting the scalar potential ϕ in Eq. (2.92) and the vector potential component ψ_z in Eq. (2.93) into Eqs. (2.96) and (2.97), the displacement components are expressed as follows, where A_5 A_6, B_5, and B_6 are coefficients,

$$u_r = e^{i(kb\theta-\omega t)} \cdot \begin{Bmatrix} \frac{\omega}{2c_1}\left[J_{kb-1}\left(\frac{\omega r}{c_1}\right) - J_{kb+1}\left(\frac{\omega r}{c_1}\right)\right] A_5 \\ \frac{\omega}{2c_1}\left[Y_{kb-1}\left(\frac{\omega r}{c_1}\right) - Y_{kb+1}\left(\frac{\omega r}{c_1}\right)\right] A_6 \\ \frac{ikb}{r} J_{kb}\left(\frac{\omega r}{c_2}\right) B_5 \\ \frac{ikb}{r} Y_{kb}\left(\frac{\omega r}{c_2}\right) B_6 \end{Bmatrix} \tag{2.99}$$

$$u_\theta = e^{i(kb\theta-\omega t)} \cdot \begin{Bmatrix} \frac{ikb}{r} J_{kb}\left(\frac{\omega r}{c_1}\right) A_5 \\ \frac{ikb}{r} Y_{kb}\left(\frac{\omega r}{c_1}\right) A_6 \\ -\frac{\omega}{2c_2}\left[J_{kb-1}\left(\frac{\omega r}{c_2}\right) - J_{kb+1}\left(\frac{\omega r}{c_2}\right)\right] B_5 \\ -\frac{\omega}{2c_2}\left[Y_{kb-1}\left(\frac{\omega r}{c_2}\right) - Y_{kb+1}\left(\frac{\omega r}{c_2}\right)\right] B_6 \end{Bmatrix} \tag{2.100}$$

The strain components in the cylindrical coordinates can then be found using the strain and displacement relations.

$$\varepsilon_{rr} = \frac{\partial u_r}{\partial r} = \left(g'' + \frac{ikb}{r} h' - \frac{ikb}{r^2} h \right) e^{i(kb\theta - \omega t)} \tag{2.101}$$

$$\varepsilon_{\theta\theta} = \frac{1}{r}\frac{\partial u_\theta}{\partial \theta} + \frac{u_r}{r} = \left(\frac{-k^2 b^2}{r^2} g + \frac{1}{r} g' + \frac{ikb}{r^2} h - \frac{ikb}{r} h' \right) e^{i(kb\theta - \omega t)} \tag{2.102}$$

$$\varepsilon_{zz} = \frac{\partial u_z}{\partial z} = 0 \tag{2.103}$$

$$\begin{aligned} \varepsilon_{r\theta} &= \frac{1}{2}\left(\frac{1}{r}\frac{\partial u_r}{\partial \theta} + \frac{\partial u_\theta}{\partial r} - \frac{u_\theta}{r} \right) \\ &= \frac{1}{2}\left(\frac{2ikb}{r} g' - \frac{2ikb}{r^2} g - h'' + \frac{1}{r} h' - \frac{k^2 b^2}{r^2} h \right) e^{i(kb\theta - \omega t)} \end{aligned} \tag{2.104}$$

$$\varepsilon_{rz} = \frac{1}{2}\left(\frac{\partial u_z}{\partial r} + \frac{\partial u_r}{\partial z} \right) = 0 \tag{2.105}$$

$$\varepsilon_{\theta z} = \frac{1}{2}\left(\frac{\partial u_\theta}{\partial z} + \frac{1}{r}\frac{\partial u_z}{\partial \theta} \right) = 0 \tag{2.106}$$

Substituting Eqs. (2.99) and (2.100) into Eqs. (2.101) and (2.104), the strain components ε_{rr} and $\varepsilon_{r\theta}$ can be defined using coefficients A_5 A_6, B_5, and B_6,

$$\varepsilon_{rr} = e^{(ikb\theta-\omega t)} \cdot \begin{Bmatrix} \left[\begin{matrix} \frac{\omega(kb-1)}{2c_1 r} J_{kb-1}\left(\frac{\omega r}{c_1}\right) - \frac{\omega^2}{c_1^2} J_{kb}\left(\frac{\omega r}{c_1}\right) \\ + \frac{\omega(kb+1)}{2c_1 r} J_{kb+1}\left(\frac{\omega r}{c_1}\right) \end{matrix}\right] A_5 \\ \left[\begin{matrix} \frac{\omega(kb-1)}{2c_1 r} Y_{kb-1}\left(\frac{\omega r}{c_1}\right) - \frac{\omega^2}{c_1^2} Y_{kb}\left(\frac{\omega r}{c_1}\right) \\ + \frac{\omega(kb+1)}{2c_1 r} Y_{kb+1}\left(\frac{\omega r}{c_1}\right) \end{matrix}\right] A_6 \\ \left[\frac{ikb\omega}{2c_2 r}\left(J_{kb-1}\left(\frac{\omega r}{c_2}\right) - J_{kb+1}\left(\frac{\omega r}{c_2}\right)\right) - \frac{ikb}{r^2} J_{kb}\left(\frac{\omega r}{c_2}\right)\right] B_5 \\ \left[\frac{ikb\omega}{2c_2 r}\left(Y_{kb-1}\left(\frac{\omega r}{c_2}\right) - Y_{kb+1}\left(\frac{\omega r}{c_2}\right)\right) - \frac{ikb}{r^2} Y_{kb}\left(\frac{\omega r}{c_2}\right)\right] B_6 \end{Bmatrix} \tag{2.107}$$

$$\varepsilon_{r\theta} = e^{(ikb\theta-\omega t)} \cdot \begin{Bmatrix} \left[\frac{ikb\omega}{2c_1 r}\left(J_{kb-1}\left(\frac{\omega r}{c_1}\right) - J_{kb+1}\left(\frac{\omega r}{c_1}\right)\right) - \frac{ikb}{r^2} J_{kb}\left(\frac{\omega r}{c_1}\right)\right] A_5 \\ \left[\frac{ikb\omega}{2c_1 r}\left(Y_{kb-1}\left(\frac{\omega r}{c_1}\right) - Y_{kb+1}\left(\frac{\omega r}{c_1}\right)\right) - \frac{ikb}{r^2} Y_{kb}\left(\frac{\omega r}{c_1}\right)\right] A_6 \\ \frac{1}{2}\left[\begin{matrix} \frac{\omega(2-kb)}{2c_2 r} J_{kb-1}\left(\frac{\omega r}{c_2}\right) + \left(\frac{\omega^2}{c_2^2} - \frac{k^2 b^2}{r^2}\right) J_{kb}\left(\frac{\omega r}{c_2}\right) \\ - \frac{\omega(kb+2)}{2c_2 r} J_{kb+1}\left(\frac{\omega r}{c_2}\right) \end{matrix}\right] B_5 \\ \frac{1}{2}\left[\begin{matrix} \frac{\omega(2-kb)}{2c_2 r} Y_{kb-1}\left(\frac{\omega r}{c_2}\right) + \left(\frac{\omega^2}{c_2^2} - \frac{k^2 b^2}{r^2}\right) Y_{kb}\left(\frac{\omega r}{c_2}\right) \\ - \frac{\omega(kb+2)}{2c_2 r} Y_{kb+1}\left(\frac{\omega r}{c_2}\right) \end{matrix}\right] B_6 \end{Bmatrix} \tag{2.108}$$

Finally, using the Hooke's law defined in Eqs. (2.34) and (2.35) along with the stress-strain relation, the stress components σ_{rr} and $\sigma_{r\theta}$ can be found as Eqs. (2.109) and (2.110).

$$\sigma_{rr} = e^{(ikb\theta-\omega t)} \cdot \begin{Bmatrix} \left[\begin{array}{l} \dfrac{\omega(\lambda+2\mu)kb-2\mu}{2c_1 r} J_{kb-1}\left(\dfrac{\omega r}{c_1}\right) \\ +\left[-(\lambda+2\mu)\dfrac{\omega^2}{c_1^2}-\lambda\dfrac{k^2b^2}{r^2}\right] J_{kb}\left(\dfrac{\omega r}{c_1}\right) \\ +\dfrac{\omega(\lambda+2\mu)kb+2\mu}{2c_1 r} J_{kb+1}\left(\dfrac{\omega r}{c_1}\right) \end{array} \right] A_5 \\ \left[\begin{array}{l} \dfrac{\omega(\lambda+2\mu)kb-2\mu}{2c_1 r} Y_{kb-1}\left(\dfrac{\omega r}{c_1}\right) \\ +\left[-(\lambda+2\mu)\dfrac{\omega^2}{c_1^2}-\lambda\dfrac{k^2b^2}{r^2}\right] Y_{kb}\left(\dfrac{\omega r}{c_1}\right) \\ +\dfrac{\omega(\lambda+2\mu)kb+2\mu}{2c_1 r} Y_{kb+1}\left(\dfrac{\omega r}{c_1}\right) \end{array} \right] A_6 \\ 2\mu\left[\dfrac{ikb\omega}{2c_2 r}\left(J_{kb-1}\left(\dfrac{\omega r}{c_2}\right)-J_{kb+1}\left(\dfrac{\omega r}{c_2}\right)\right)-\dfrac{ikb}{r^2}J_{kb}\left(\dfrac{\omega r}{c_2}\right)\right] B_5 \\ 2\mu\left[\dfrac{ikb\omega}{2c_2 r}\left(Y_{kb-1}\left(\dfrac{\omega r}{c_2}\right)-Y_{kb+1}\left(\dfrac{\omega r}{c_2}\right)\right)-\dfrac{ikb}{r^2}Y_{kb}\left(\dfrac{\omega r}{c_2}\right)\right] B_6 \end{Bmatrix} \tag{2.109}$$

$$\sigma_{r\theta} = e^{(ikb\theta-\omega t)}.\begin{Bmatrix} 2\mu\left[\frac{ikb\omega}{2c_1 r}\left(J_{kb-1}\left(\frac{\omega r}{c_1}\right)-J_{kb+1}\left(\frac{\omega r}{c_1}\right)\right)-\frac{ikb}{r^2}J_{kb}\left(\frac{\omega r}{c_1}\right)\right]A_5 \\ 2\mu\left[\frac{ikb\omega}{2c_1 r}\left(Y_{kb-1}\left(\frac{\omega r}{c_1}\right)-Y_{kb+1}\left(\frac{\omega r}{c_1}\right)\right)-\frac{ikb}{r^2}Y_{kb}\left(\frac{\omega r}{c_1}\right)\right]A_6 \\ \mu\left[\begin{array}{l}\frac{\omega(2-kb)}{2c_2 r}J_{kb-1}\left(\frac{\omega r}{c_2}\right)+\left(\frac{\omega^2}{c_2^2}-\frac{k^2b^2}{r^2}\right)J_{kb}\left(\frac{\omega r}{c_2}\right) \\ -\frac{\omega(kb+2)}{2c_2 r}J_{kb+1}\left(\frac{\omega r}{c_2}\right)\end{array}\right]B_5 \\ \mu\left[\begin{array}{l}\frac{\omega(2-kb)}{2c_2 r}Y_{kb-1}\left(\frac{\omega r}{c_2}\right)+\left(\frac{\omega^2}{c_2^2}-\frac{k^2b^2}{r^2}\right)Y_{kb}\left(\frac{\omega r}{c_2}\right) \\ -\frac{\omega(kb+2)}{2c_2 r}Y_{kb+1}\left(\frac{\omega r}{c_2}\right)\end{array}\right]B_6 \end{Bmatrix} \quad (2.110)$$

Boundary conditions are applied next to construct the global matrix. For the present problem the exposed inner and outer layers are both traction-free. Interfacial continuity condition requires that the strains and displacements along the two interfacial layers to be continuous for a perfect bond.

The stress-free surface boundary conditions are therefore

$$\begin{Bmatrix}\sigma_{rr}\\ \sigma_{r\theta}\end{Bmatrix}_{surface} = 0 \quad (2.111)$$

In vector form the stress for a single layer is

$$\begin{Bmatrix}\sigma_{rr}\\ \sigma_{r\theta}\end{Bmatrix} = [D_5]\begin{Bmatrix}A_5\\ A_6\\ B_5\\ B_6\end{Bmatrix} \quad (2.112)$$

The interfacial boundary condition requires that the displacement and strain fields are continuous at the interface of the two bonding materials, thus the followings

$$\left\{\begin{matrix} u_r \\ u_\theta \\ \varepsilon_{rr} \\ \varepsilon_{r\theta} \end{matrix}\right\}_{\substack{layer\ \mathrm{p} \\ \mathrm{Interface\ p+1}}} = \left\{\begin{matrix} u_r \\ u_\theta \\ \varepsilon_{rr} \\ \varepsilon_{r\theta} \end{matrix}\right\}_{\substack{layer\ \mathrm{p+1} \\ \mathrm{Interface\ p+1}}} \tag{2.113}$$

In vector form the strain and displacement for a single layer are

$$\left\{\begin{matrix} u_r \\ u_\theta \\ \varepsilon_{rr} \\ \varepsilon_{r\theta} \end{matrix}\right\} = \left[D_6\right] \left\{\begin{matrix} A_5 \\ A_6 \\ B_5 \\ B_6 \end{matrix}\right\} \tag{2.114}$$

The layer matrix $[D_5]$ is given in Eq. (2.115). The layer matrix $[D_6]$ is defined using the inner layer matrix $[D_{6,\mathrm{i}}]$ and outer layer matrix $[D_{6,\mathrm{o}}]$ as shown in Eqs. (2.116) and (2.117). It is again noted that the subscript "i" denotes the inner position of each layer while the subscript "o" denotes the outer position of each layer.

$$
[D_5] = \begin{bmatrix}
\begin{bmatrix}
\dfrac{\omega(\lambda+2\mu)kb-2\mu}{2c_1 r} J_{kb-1}\left(\dfrac{\omega r}{c_1}\right) \\
+\left[-(\lambda+2\mu)\dfrac{\omega^2}{c_1^2}-\lambda\dfrac{k^2b^2}{r^2}\right] J_{kb}\left(\dfrac{\omega r}{c_1}\right) \\
+\dfrac{\omega(\lambda+2\mu)kb+2\mu}{2c_1 r} J_{kb+1}\left(\dfrac{\omega r}{c_1}\right)
\end{bmatrix} &
\begin{bmatrix}
\dfrac{\omega(\lambda+2\mu)kb-2\mu}{2c_1 r} Y_{kb-1}\left(\dfrac{\omega r}{c_1}\right) \\
+\left[-(\lambda+2\mu)\dfrac{\omega^2}{c_1^2}-\lambda\dfrac{k^2b^2}{r^2}\right] Y_{kb}\left(\dfrac{\omega r}{c_1}\right) \\
+\dfrac{\omega(\lambda+2\mu)kb+2\mu}{2c_1 r} Y_{kb+1}\left(\dfrac{\omega r}{c_1}\right)
\end{bmatrix} &
\begin{bmatrix}
\dfrac{i\mu kb\omega}{c_2 r}\left(J_{kb-1}\left(\dfrac{\omega r}{c_2}\right)-J_{kb+1}\left(\dfrac{\omega r}{c_2}\right)\right) \\
-\dfrac{2i\mu kb}{r^2} J_{kb}\left(\dfrac{\omega r}{c_2}\right)
\end{bmatrix} &
\begin{bmatrix}
\dfrac{i\mu kb\omega}{c_2 r}\left(Y_{kb-1}\left(\dfrac{\omega r}{c_2}\right)-Y_{kb+1}\left(\dfrac{\omega r}{c_2}\right)\right) \\
-\dfrac{2i\mu kb}{r^2} Y_{kb}\left(\dfrac{\omega r}{c_2}\right)
\end{bmatrix} \\
\begin{bmatrix}
\dfrac{i\mu kb\omega}{c_1 r}\left(J_{kb-1}\left(\dfrac{\omega r}{c_1}\right)-J_{kb+1}\left(\dfrac{\omega r}{c_1}\right)\right) \\
-\dfrac{2i\mu kb}{r^2} J_{kb}\left(\dfrac{\omega r}{c_1}\right)
\end{bmatrix} &
\begin{bmatrix}
\dfrac{i\mu kb\omega}{c_1 r}\left(Y_{kb-1}\left(\dfrac{\omega r}{c_1}\right)-Y_{kb+1}\left(\dfrac{\omega r}{c_1}\right)\right) \\
-\dfrac{2i\mu kb}{r^2} Y_{kb}\left(\dfrac{\omega r}{c_1}\right)
\end{bmatrix} &
\mu\begin{bmatrix}
\dfrac{\omega(2-kb)}{2c_2 r} J_{kb-1}\left(\dfrac{\omega r}{c_2}\right) \\
+\left(\dfrac{\omega^2}{c_2^2}-\dfrac{k^2b^2}{r^2}\right) J_{kb}\left(\dfrac{\omega r}{c_2}\right) \\
-\dfrac{\omega(kb+2)}{2c_2 r} J_{kb+1}\left(\dfrac{\omega r}{c_2}\right)
\end{bmatrix} &
\mu\begin{bmatrix}
\dfrac{\omega(2-kb)}{2c_2 r} Y_{kb-1}\left(\dfrac{\omega r}{c_2}\right) \\
+\left(\dfrac{\omega^2}{c_2^2}-\dfrac{k^2b^2}{r^2}\right) Y_{kb}\left(\dfrac{\omega r}{c_2}\right) \\
-\dfrac{\omega(kb+2)}{2c_2 r} Y_{kb+1}\left(\dfrac{\omega r}{c_2}\right)
\end{bmatrix}
\end{bmatrix}
$$

(2.115)

$$
\left[D_{6,i}\right]=\begin{bmatrix}
\dfrac{\omega}{2c_1}\left[J_{kb-1}\left(\dfrac{\omega r_i}{c_1}\right)-J_{kb+1}\left(\dfrac{\omega r_i}{c_1}\right)\right] & \dfrac{\omega}{2c_1}\left[Y_{kb-1}\left(\dfrac{\omega r_i}{c_1}\right)-Y_{kb+1}\left(\dfrac{\omega r_i}{c_1}\right)\right] & \dfrac{ikb}{r_i}J_{kb}\left(\dfrac{\omega r_i}{c_2}\right) & \dfrac{ikb}{r_i}Y_{kb}\left(\dfrac{\omega r_i}{c_2}\right) \\
\dfrac{ikb}{r_i}J_{kb}\left(\dfrac{\omega r_i}{c_1}\right) & \dfrac{ikb}{r_i}Y_{kb}\left(\dfrac{\omega r_i}{c_1}\right) & -\dfrac{\omega}{2c_2}\left[J_{kb-1}\left(\dfrac{\omega r_i}{c_2}\right)-J_{kb+1}\left(\dfrac{\omega r_i}{c_2}\right)\right] & -\dfrac{\omega}{2c_2}\left[Y_{kb-1}\left(\dfrac{\omega r_i}{c_2}\right)-Y_{kb+1}\left(\dfrac{\omega r_i}{c_2}\right)\right] \\
\left[\begin{matrix}\dfrac{\omega(kb-1)}{2c_1r_i}J_{kb-1}\left(\dfrac{\omega r_i}{c_1}\right)-\dfrac{\omega^2}{c_1^2}J_{kb}\left(\dfrac{\omega r_i}{c_1}\right)\\ +\dfrac{\omega(kb+1)}{2c_1r_i}J_{kb+1}\left(\dfrac{\omega r_i}{c_1}\right)\end{matrix}\right] & \left[\begin{matrix}\dfrac{\omega(kb-1)}{2c_1r_i}Y_{kb-1}\left(\dfrac{\omega r_i}{c_1}\right)-\dfrac{\omega^2}{c_1^2}Y_{kb}\left(\dfrac{\omega r_i}{c_1}\right)\\ +\dfrac{\omega(kb+1)}{2c_1r_i}Y_{kb+1}\left(\dfrac{\omega r_i}{c_1}\right)\end{matrix}\right] & \left[\begin{matrix}\dfrac{ikb\omega}{2c_2r_i}\left(J_{kb-1}\left(\dfrac{\omega r_i}{c_2}\right)-J_{kb+1}\left(\dfrac{\omega r_i}{c_2}\right)\right)\\ -\dfrac{ikb}{r_i^2}J_{kb}\left(\dfrac{\omega r_i}{c_2}\right)\end{matrix}\right] & \left[\begin{matrix}\dfrac{ikb\omega}{2c_2r_i}\left(Y_{kb-1}\left(\dfrac{\omega r_i}{c_2}\right)-Y_{kb+1}\left(\dfrac{\omega r_i}{c_2}\right)\right)\\ -\dfrac{ikb}{r_i^2}Y_{kb}\left(\dfrac{\omega r_i}{c_2}\right)\end{matrix}\right] \\
\left[\begin{matrix}\dfrac{ikb\omega}{2c_1r_i}\left(J_{kb-1}\left(\dfrac{\omega r_i}{c_1}\right)-J_{kb+1}\left(\dfrac{\omega r_i}{c_1}\right)\right)\\ -\dfrac{ikb}{r_i^2}J_{kb}\left(\dfrac{\omega r_i}{c_1}\right)\end{matrix}\right] & \left[\begin{matrix}\dfrac{ikb\omega}{2c_1r_i}\left(Y_{kb-1}\left(\dfrac{\omega r_i}{c_1}\right)-Y_{kb+1}\left(\dfrac{\omega r_i}{c_1}\right)\right)\\ -\dfrac{ikb}{r_i^2}Y_{kb}\left(\dfrac{\omega r_i}{c_1}\right)\end{matrix}\right] & \dfrac{1}{2}\left[\begin{matrix}\dfrac{\omega(2-kb)}{2c_2r_i}J_{kb-1}\left(\dfrac{\omega r_i}{c_2}\right)\\ +\left(\dfrac{\omega^2}{c_2^2}-\dfrac{k^2b^2}{r_i^2}\right)J_{kb}\left(\dfrac{\omega r_i}{c_2}\right)\\ -\dfrac{\omega(kb+2)}{2c_2r_i}J_{kb+1}\left(\dfrac{\omega r_i}{c_2}\right)\end{matrix}\right] & \dfrac{1}{2}\left[\begin{matrix}\dfrac{\omega(2-kb)}{2c_2r_i}Y_{kb-1}\left(\dfrac{\omega r_i}{c_2}\right)\\ +\left(\dfrac{\omega^2}{c_2^2}-\dfrac{k^2b^2}{r_i^2}\right)Y_{kb}\left(\dfrac{\omega r_i}{c_2}\right)\\ -\dfrac{\omega(kb+2)}{2c_2r_i}Y_{kb+1}\left(\dfrac{\omega r_i}{c_2}\right)\end{matrix}\right]
\end{bmatrix}
$$

(2.116)

$$
\left[D_{6,o}\right]=\begin{bmatrix}
\frac{\omega}{2c_1}\left[J_{kb-1}\left(\frac{\omega r_o}{c_1}\right)-J_{kb+1}\left(\frac{\omega r_o}{c_1}\right)\right] & \frac{\omega}{2c_1}\left[Y_{kb-1}\left(\frac{\omega r_o}{c_1}\right)-Y_{kb+1}\left(\frac{\omega r_o}{c_1}\right)\right] & \frac{ikb}{r_o}J_{kb}\left(\frac{\omega r_o}{c_2}\right) & \frac{ikb}{r_o}Y_{kb}\left(\frac{\omega r_o}{c_2}\right) \\
\frac{ikb}{r_o}J_{kb}\left(\frac{\omega r_o}{c_1}\right) & \frac{ikb}{r_o}Y_{kb}\left(\frac{\omega r_o}{c_1}\right) & -\frac{\omega}{2c_2}\left[J_{kb-1}\left(\frac{\omega r_o}{c_2}\right)-J_{kb+1}\left(\frac{\omega r_o}{c_2}\right)\right] & -\frac{\omega}{2c_2}\left[Y_{kb-1}\left(\frac{\omega r_o}{c_2}\right)-Y_{kb+1}\left(\frac{\omega r_o}{c_2}\right)\right] \\
\begin{bmatrix}\frac{\omega(kb-1)}{2c_1r_o}J_{kb-1}\left(\frac{\omega r_o}{c_1}\right)-\frac{\omega^2}{c_1^2}J_{kb}\left(\frac{\omega r_o}{c_1}\right)\\ +\frac{\omega(kb+1)}{2c_1r_o}J_{kb+1}\left(\frac{\omega r_o}{c_1}\right)\end{bmatrix} & \begin{bmatrix}\frac{\omega(kb-1)}{2c_1r_o}Y_{kb-1}\left(\frac{\omega r_o}{c_1}\right)-\frac{\omega^2}{c_1^2}Y_{kb}\left(\frac{\omega r_o}{c_1}\right)\\ +\frac{\omega(kb+1)}{2c_1r_o}Y_{kb+1}\left(\frac{\omega r_o}{c_1}\right)\end{bmatrix} & \begin{bmatrix}\frac{ikb\omega}{2c_2r_o}\left(J_{kb-1}\left(\frac{\omega r_o}{c_2}\right)-J_{kb+1}\left(\frac{\omega r_o}{c_2}\right)\right)\\ -\frac{ikb}{r_o^2}J_{kb}\left(\frac{\omega r_o}{c_2}\right)\end{bmatrix} & \begin{bmatrix}\frac{ikb\omega}{2c_2r_o}\left(Y_{kb-1}\left(\frac{\omega r_o}{c_2}\right)-Y_{kb+1}\left(\frac{\omega r_o}{c_2}\right)\right)\\ -\frac{ikb}{r_o^2}Y_{kb}\left(\frac{\omega r_o}{c_2}\right)\end{bmatrix} \\
\begin{bmatrix}\frac{ikb\omega}{2c_1r_o}\left(J_{kb-1}\left(\frac{\omega r_o}{c_1}\right)-J_{kb+1}\left(\frac{\omega r_o}{c_1}\right)\right)\\ -\frac{ikb}{r_o^2}J_{kb}\left(\frac{\omega r_o}{c_1}\right)\end{bmatrix} & \begin{bmatrix}\frac{ikb\omega}{2c_1r_o}\left(Y_{kb-1}\left(\frac{\omega r_o}{c_1}\right)-Y_{kb+1}\left(\frac{\omega r_o}{c_1}\right)\right)\\ -\frac{ikb}{r_o^2}Y_{kb}\left(\frac{\omega r_o}{c_1}\right)\end{bmatrix} & \frac{1}{2}\begin{bmatrix}\frac{\omega(2-kb)}{2c_2r_o}J_{kb-1}\left(\frac{\omega r_o}{c_2}\right)\\ +\left(\frac{\omega^2}{c_2^2}-\frac{k^2b^2}{r_o^2}\right)J_{kb}\left(\frac{\omega r_o}{c_2}\right)\\ -\frac{\omega(kb+2)}{2c_2r_o}J_{kb+1}\left(\frac{\omega r_o}{c_2}\right)\end{bmatrix} & \frac{1}{2}\begin{bmatrix}\frac{\omega(2-kb)}{2c_2r_o}Y_{kb-1}\left(\frac{\omega r_o}{c_2}\right)\\ +\left(\frac{\omega^2}{c_2^2}-\frac{k^2b^2}{r_o^2}\right)Y_{kb}\left(\frac{\omega r_o}{c_2}\right)\\ -\frac{\omega(kb+2)}{2c_2r_o}Y_{kb+1}\left(\frac{\omega r_o}{c_2}\right)\end{bmatrix}
\end{bmatrix}
\tag{2.117}
$$

With the layer matrices $[D_5]$, $[D_{6,i}]$, and $[D_{6,o}]$, the corresponding global matrix can be constructed. The traction-free boundary conditions require the followings to be satisfied:

$$\left[D_5\right]_i \begin{Bmatrix} A_5 \\ A_6 \\ B_5 \\ B_6 \end{Bmatrix} = \begin{Bmatrix} 0 \\ 0 \end{Bmatrix} \tag{2.118}$$

$$\left[D_5\right]_o \begin{Bmatrix} A_5 \\ A_6 \\ B_5 \\ B_6 \end{Bmatrix} = \begin{Bmatrix} 0 \\ 0 \end{Bmatrix} \tag{2.119}$$

with "i" and "o" referring to the inner and outer surfaces, respectively. Furthermore, perfectly bonded interface boundary conditions are defined as

$$\left[\left[D_{6,o}\right]_{layer=p} \left[-D_{6,i}\right]_{layer=p+1}\right] \begin{Bmatrix} A_{5,p} \\ A_{6,p} \\ B_{5,p} \\ B_{6,p} \\ A_{5,p+1} \\ A_{6,p+1} \\ B_{5,p+1} \\ B_{6,p+1} \end{Bmatrix} = \begin{Bmatrix} 0 \\ 0 \\ 0 \\ 0 \\ 0 \\ 0 \\ 0 \\ 0 \end{Bmatrix} \tag{2.120}$$

Combining Eqs. (2.118)-(2.120), and using a two-layer model as an example, the global matrix equation is then

$$\begin{bmatrix} [D_5]_i & 0 \\ [D_{6,o}]_{layer=1} & [-D_{6,i}]_{layer=2} \\ 0 & [D_5]_o \end{bmatrix} \begin{Bmatrix} A_{5,1} \\ A_{6,1} \\ B_{5,1} \\ B_{6,1} \\ A_{5,2} \\ A_{6,2} \\ B_{5,2} \\ B_{6,2} \end{Bmatrix} = \begin{Bmatrix} \{0\} \\ \{0\} \end{Bmatrix} \tag{2.121}$$

The corresponding characteristic dispersion equation for the circumferential longitudinal wave can be obtained by setting the following determinant to zero:

$$\det\left(\begin{vmatrix} [D_1]_i & 0 \\ [D_{1,o}]_{layer=1} & [-D_{2,i}]_{layer=2} \\ 0 & [D_1]_o \end{vmatrix} \right) = 0 \tag{2.122}$$

Using Eq. (2.122), the dispersion of the circumferentially running longitudinal wave can be determined by plotting the phase velocity as a function of the frequency. A numerical scheme is adopted in Sec. 4 to perform this particular task. Using the dispersion equation but replacing the real material constants with complex material constants, the impact of the viscoelasticity of the layer materials can be established.

3. CONSTITUTIVE EQUATION FOR VISCOELASTIC LAYER

Viscoelastic materials store energy when deformed and dissipate energy as time transpires. They also undergo stress relaxation and creep. Stress relaxation is a process in which the stress decreases over time while the strain remains constant. The opposite is true for creep where the strain increases while the applied stress stays constant. The Maxwell model [22] describes how stresses relax for viscoelastic materials but it does not describe creep. The Kelvin-Voight model [22] imparts viscoelastic materials with creep characteristics but falls short of explaining stress relaxation.

The viscoelastic constitutive model developed by Boltzmann [22] is more general. It begins with considering a simple bar that is subjected to a stress $\sigma(t)$ that is continuous and differential in time. The increment of the stress $\sigma(t)$ over a small time interval $d\tau$ is

$$d\sigma = \frac{d\sigma}{d\tau} d\tau \tag{3.1}$$

Boltzmann argued that the stress increment through time t depends on the strain increment $d\varepsilon$ at time τ. Furthermore, the stress relaxes over the time $(t-\tau)$ as

$$d\sigma = G_{\alpha}(t-\tau)\frac{d\varepsilon(\tau)}{d\tau} d\tau \tag{3.2}$$

where G_{α} is the modulus of the viscoelastic material with $\alpha = 1$ corresponding to the case of extensional stress and $\alpha = 2$ the case of shear stress. By integrating the stress

increment from time $-\infty$ to time t, over all increments $d\tau$, the complete stress at time t can be obtained as

$$\sigma = \int_{-\infty}^{t} \left[G_{\alpha}(t-\tau) \frac{d\varepsilon(\tau)}{d\tau} \right] d\tau \tag{3.3}$$

It was assumed in the previous section that the guided wave motions are time-harmonic motion and in steady state. The motions of the corresponding stress and strain fields will therefore be considered to be time harmonic in the derivation that follows.

The strain that is harmonic in time is

$$\varepsilon = \varepsilon_0 e^{i\omega t} \tag{3.4}$$

where ε_0 is the oscillation amplitude and ω is the frequency. In Eq. (3.5), G_{α} is separated into two parts. One is a constant $G_{\alpha,c}$ and the other is a time-varying $G_{\alpha,t}(t)$.

$$G_{\alpha}(t) = G_{\alpha,c} + G_{\alpha,t}(t) \tag{3.5}$$

Substituting Eqs. (3.4) and (3.5) into (3.3), we have

$$\sigma(t) = G_{\alpha,c}\varepsilon_0 e^{i\omega t} + i\omega\varepsilon_0 \int_{-\infty}^{t} G_{\alpha,t}(t-\tau) e^{i\omega\tau} d\tau \tag{3.6}$$

Using $t-\tau = \eta$ and decomposing the exponential function into the corresponding sine and cosine functions, Eq. (3.6) can be recast into

$$\sigma(t) = \left[G_{\alpha,c} + \omega \int_{-\infty}^{t} G_{\alpha,t}(\eta) \cdot \sin(\omega\eta)\, d\tau + i\omega \int_{-\infty}^{t} G_{\alpha,t}(\eta) \cdot \cos(\omega\eta)\, d\tau \right] \varepsilon_0 e^{i\omega t} \tag{3.7}$$

Letting

$$G_{\alpha,c} + \omega \int_{-\infty}^{t} G_{\alpha,t}(\eta) \cdot \sin(\omega\eta)\, d\tau + i\omega \int_{-\infty}^{t} G_{\alpha,t}(\eta) \cdot \cos(\omega\eta)\, d\tau = G_{\alpha} * (i\omega) \tag{3.8}$$

Eq. (3.7) can be simplified using Eqs. (3.8) and (3.4)

$$\sigma(t) = G_\alpha * (i\omega)\varepsilon_0 e^{i\omega t} = G_\alpha * (i\omega)\varepsilon(t) \tag{3.9}$$

Eq. (3.9) suggests that the stress-strain constitutive relationship for viscoelastic materials can be formulated by employing complex viscoelastic moduli that are frequency dependent. In other words, material viscoelasticity can be addressed simply by considering complex material constitutive law. The correspondence principle [23] describes this substitution of real material property with the complex one to account for viscoelastic response for the time harmonic case. In the Section that follows, the elastic constants of the coating layers for the time harmonic elastic solution are replaced by their viscoelastic counterparts to investigate the effect of the coating materials on wave dispersion and attenuation. Specifically the harmonic wave propagation in the tubular section with viscoelastic coatings are explored by replacing the real Lame constants with complex, viscoelastic Lame constants μ^* and λ^* in the Navier equation of motion as,

$$\mu^*\nabla^2 u + (\lambda^* + \mu^*)\nabla(\nabla \cdot u) = \rho(\partial^2 u / \partial^2 t) \tag{3.10}$$

The same derivations detailed in the previous sections can be followed and the same boundary conditions can be applied to generate the dispersion equations for the guided modes in tubing coated with viscoelastic thin layers.

4. NUMERICAL RESULTS AND DISCUSSION

Since analytical solutions are not available for the dispersion equations derived for the viscoelastically coated tubing, numerical solutions have to be sought. Material constants to be employed are determined by the materials used for the tubular and coating. The objective of the numerical procedure is therefore to determine the frequency, ω, as a function of the wavenumber, k. Roots thus obtained can be manipulated to allow phase velocity and attenuation dispersion to be plotted against frequency – the two fundamental characteristics of any propagating wave.

The presence of viscoelastic coatings necessarily renders the roots of the dispersion equation complex. When the roots of a wave solution are real, the wave propagates with no attenuation. Waves whose dispersion roots are complex will be attenuated in time and space. As such it is expected that guided waves are both dispersive and attenuative as they propagate in elastic tubing with viscoelastic coatings. Furthermore, the number of roots at each frequency is not constant. Generally the number increases as the frequency goes higher.

The numerical routine formulated to find the complex roots is described below. Numerical results associated with the three guided modes considered, namely, the longitudinal wave along the axial direction, and the shear and longitudinal waves along the circumferential direction are then presented.

4.1. Bisection Method and Numerical Routine for Finding Complex Roots

There are many numerical methods available to solve for roots of an equation. Few of the popular methods are Newton-Raphson method, Bisection method and Secant Method. Newton-Raphson method and Secant method have the disadvantage that they need a good initial guess to approach the roots which are not suitable for the study at hand. Since the system for the elastic cylinder have only real roots and the solution of the dispersion equation is multi-valued, bisection method is adopted to solve for the roots of the wave dispersion. The bisection method is also known as the interval having method. In bisection method, for a particular frequency, ω , the signs of the determinants related to two different phase velocities, a and b, are opposite. There must exist at least one root between a and b. To make sure there is only one root inside the range of (a, b), the interval must be chosen to be small enough. After inserting an e which is the mid-value of a and b, the sign of the determinant of e is then determined. If the sign of the determinant of a is different from the sign of the determinant of e, then a and e are considered as the new interval for search. Otherwise, b and e are the new interval. This iteration process continues until the interval or the determinant become small enough to indicate the convergence to a root.

If the model is composed of only elastic materials, the wave number solution will be in the real domain. By using the bisection method all the roots of the characteristic dispersion equation for the elastic model can be found since the behaviors of the waves are harmonic [24]. Thus, the phase velocity dispersion curve can be plotted for the tubing models of guided wave generation introduced in Sec. 2.

Now that the root-search routine for elastic models is developed, the next is to modify the search routine to find the roots for the wave dispersion equation of an elastic tubular with multiple viscoelastic coatings. As the roots are complex, a complex root finding algorithm will be needed. The wave number now has a real part and an imaginary part as follows

$$k = \mathrm{Re}(k) + i\,\mathrm{Im}(k) \tag{4.1}$$

The imaginary part of the wave number defines the attenuation while the real part along with the frequency describes the phase velocity as

$$c_{ph} = \frac{\omega}{\mathrm{Re}(k)} \tag{4.2}$$

$$\alpha = \mathrm{Im}(k) \tag{4.3}$$

Thus giving the wave number an alternative expression

$$k = \frac{\omega}{c_{ph}} + i\alpha \tag{4.4}$$

Using Eq. (4.4), the phase velocity and attenuation dispersion curves can be generated directly. To use the search routine efficiently to find complex roots, good initial guesses are required. The real part of the initial guess must be sufficiently close to where the value of the dispersion equation function is minimal. The hypothesis that the phase velocity of the elastic dispersion equation is close to its complex counterpart in the viscoelastic case is utilized. The real roots found in the bare (without viscoelastic coating layer) tubing case are employed as the initial guesses to search for the admissible complex roots that give the minimal norms of the determinant equation. In other words,

the search algorithm performs simultaneous search for the phase velocity and attenuation pairs as the roots of the viscoelastic dispersion equation.

Once the roots are found for all frequencies of interest, the phase velocity and attenuation dispersion curves can be plotted. Since the order of magnitude of the attenuation α varies, it is common to express α in decibels per meter as follows

$$Attenuation\left(dB/m\right)=20\log_{10}\left(e^{-1000\alpha}\right) \tag{4.5}$$

Using the above, the fundamental propagation characteristics of the three kinds of guided waves can be found for the elastic tubular section coated with thin viscoelastic layers. However, to demonstrate that the effect of the viscoelastic coatings on wave attenuation is significant, it is required that the solutions to the wave equations be obtained by solving Bessel functions of complex order – a task that is computationally demanding and numerically intensive.

4.2. Numerical Results of Longitudinal Guided Wave along Axial Direction

A schedule 40 elastic steel pipe with viscoelastic coatings is considered in the followings. The radius and thickness of the pipe are 2.25" and 0.1185", respectively. The thickness of the viscoelastic material is 0.02". The properties of the elastic tubular and the viscoelastic material can be found in [19] and [25]. The steel tubular has a density of 7.8 gm/cm^3 and the longitudinal and shear wave velocities it supports are c_1 = 5.9 km/sec and c_2 = 3.19 km/sec, respectively. Complex viscoelastic material constants that are also frequency dependent [26], on the other hand, are not readily available.

Below is the one dimensional wave propagation equation [27]

$$\frac{d^2u}{dx^2} = \frac{1}{C_\beta{}^2}\frac{d^2u}{dt^2} \tag{4.6}$$

where subscript β is either 1 for longitudinal velocity or 2 for shear velocity. The correspondence principle ensures that Eq. (4.6) also works for viscoelastic materials in which the viscoelastic constants λ^* and μ^* are the complex counterparts of the Lame constants λ and μ. Velocity C_β is therefore necessarily complex as below

$$\frac{1}{C_\beta} = \mathrm{Re}\left(\frac{1}{C_\beta}\right) + i\,\mathrm{Im}\left(\frac{1}{C_\beta}\right) \tag{4.7}$$

where the real and imaginary parts are recast using two more parameters:

$$c_\beta(\omega) = \left(\mathrm{Re}\left(\frac{1}{C_\beta}\right)\right)^{-1} \tag{4.8}$$

$$\alpha_\beta(\omega) = \omega\,\mathrm{Im}\left(\frac{1}{C_\beta}\right) \tag{4.9}$$

Substitute Eqs. (4.8) and (4.9) into Eq. (4.7), the complex wave velocity C_β is

$$C_\beta{}^*(i\omega) = \left[\frac{1}{c_\beta(\omega)} + i\frac{\alpha_\beta(\omega)}{\omega}\right]^{-1} \tag{4.10}$$

Table 4.1 tabulates the experimentally determined c_1, c_2, α_1 and α_2 for a type of E&C 2057 Epoxy coating [19], whose density is 1.6 gm/cm^3.

Table 4.1 Material Properties of E&C 2057 Epoxy [19]

c_1	c_2	α_1 / ω	α_2 / ω
2.96 (km/sec)	1.45 (km/sec)	4.7×10^{-9} (sec/m)	6.9×10^{-9} (sec/m)

Over the frequency range of interest, the velocity c_β is constant. In other words, the material properties are independent of the frequency. Furthermore, the attenuation constants α_β will be constant over the frequency range of interest if they are divided by the frequency. These conditions render the root search less demanding.

Following the steps described above and incorporating relevant material properties, the phase velocity dispersion of the longitudinal wave propagated in the bare tubular along the axial direction is obtained and shown in Fig. 4.1.

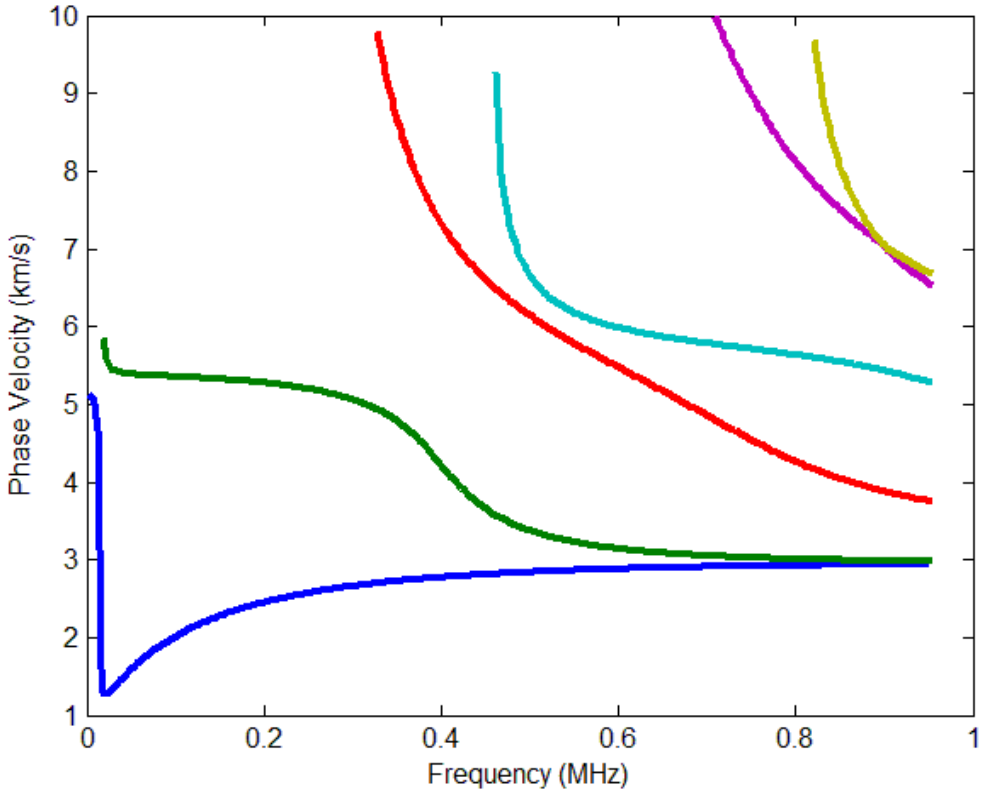

Fig. 4.1 Phase velocity dispersion curve of axial longitudinal wave in bare tubing

The phase velocity dispersion curve agrees well with the experimental results found in [19]. Specifically there are only two admissible modes in the low frequency range. More modes are admissible at higher frequency. Although more modes can be excited at higher frequency, the fundamental modes 1 and 2 are considered the most important for applications involving lower frequency generation. Furthermore, at higher frequency, all phase velocities of the different modes are seen to converge to a mode where the phase velocity becomes independent of the frequency. This marks the most

prominent difference between the pure elastic hollow cylinder model and models with viscoelastic layers.

Figs. 4.2 and 4.3 show the phase velocity and attenuation dispersion curves of the axial longitudinal wave propagated in a tubular with a single layer of epoxy coating.

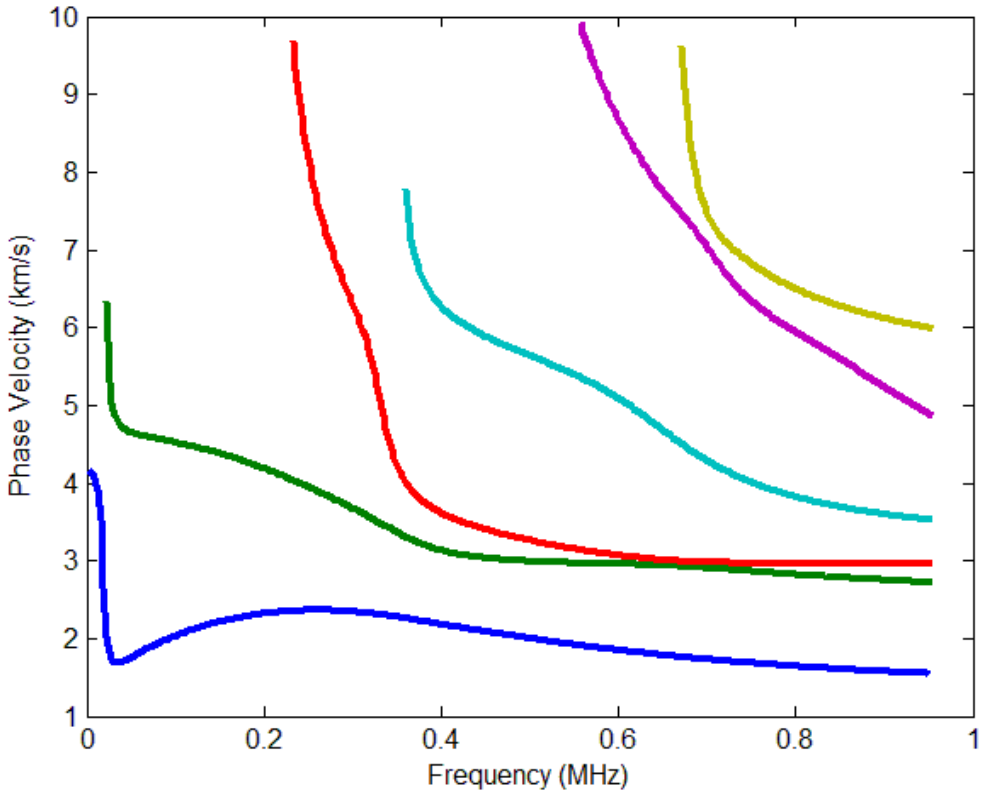

Fig. 4.2 Phase velocity dispersion curve of axial longitudinal wave in tubular with 1 epoxy layer

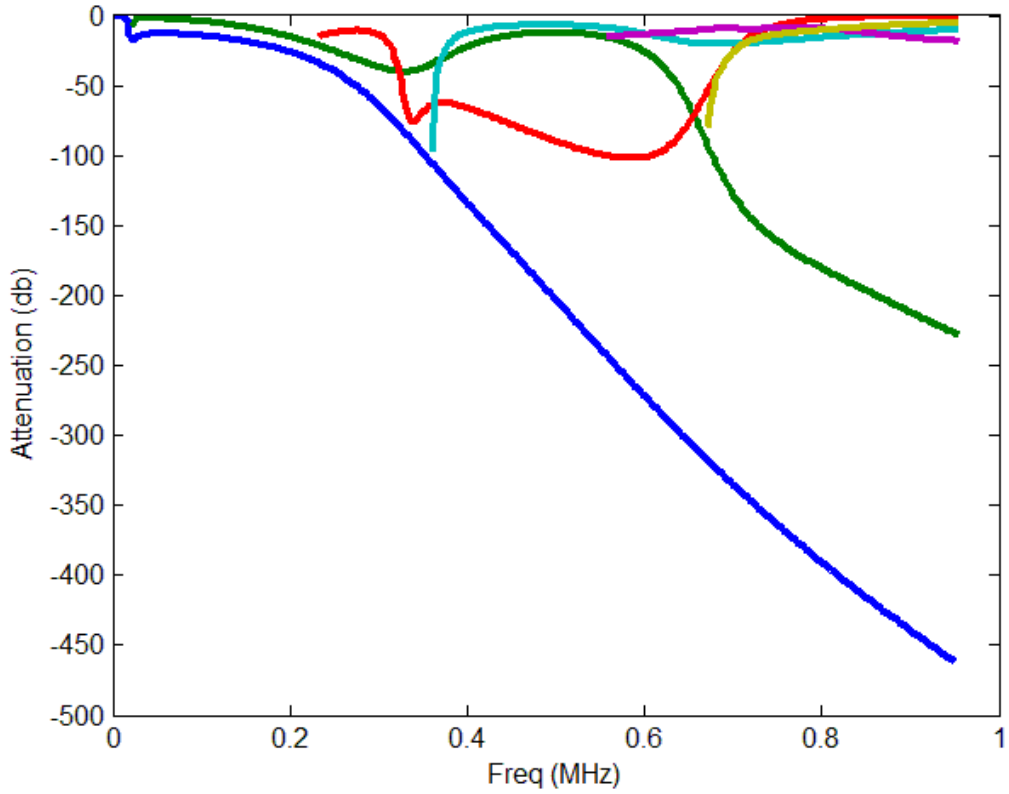

Fig. 4.3 Attenuation dispersion curve of axial longitudinal wave in tubular with 1 layer of epoxy coating

There are prominent differences between the phase velocity dispersion curves in Fig. 4.2 for the single coated layer tubular and the one corresponds to the bare tubular in Fig. 4.1. Two additional modes within the 0-0.7MHz frequency range are present in Fig. 4.2. The phase velocities associated with the 3rd and high order modes are seen to decrease much faster at frequency higher than 0.4MHz. Except for the 1st and 2nd mode, all modes converge to the same asymptotic phase velocity at 3km/s as the bare tubing case. The drastic drop of the first two modes in phase velocity is affirmed by the

corresponding attenuation dispersion curves in Fig. 4.3, in which the modes attenuate significantly at higher frequency. With such a high level of energy dissipation, the modes would not have been able to propagate far, thus explaining the deviation from the asymptotic phase velocity in Fig. 4.2. The highest three modes demonstrate negligible attenuation within the frequency range considered. This is interesting because as Eq. 4.9 indicates, the attenuation constant should increase with wave frequency. As their phase velocity resolutions would fast deteriorate at higher frequency, they may have limited engineering applications.

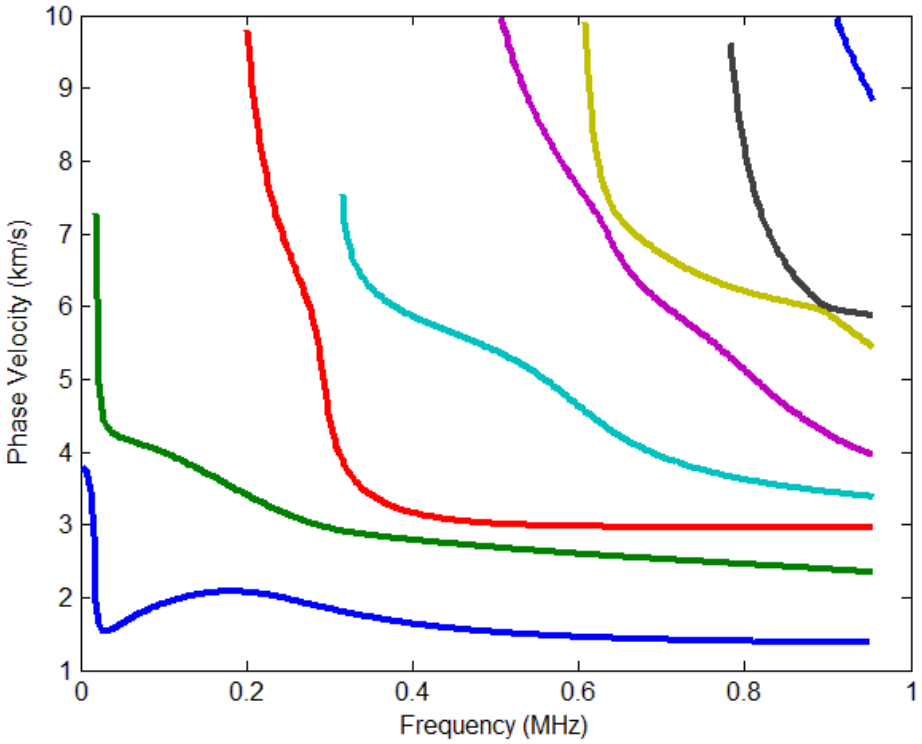

Fig. 4.4 Phase velocity dispersion curve of axial longitudinal wave in tubular with 2 epoxy layers

Wave dispersion and attenuation of the axial longitudinal wave correspond to 2 and 3 layers of viscoelastic coatings are given in Figs. 4.4-4.7. Two additional modes are seen in Fig. 4.4., in which the 3rd, 4th, and 5th mode are seen fast approaching the non-dispersive asymptotic phase velocity with poor resolution in differentiating them at frequency higher than 1.0MHz. Of all the admissible modes in Fig. 4.5, the 3rd mode demonstrates the least attenuation between 0.2 and 1.0MHz, making it a potential candidate for charactering tubing with 2 epoxy coatings. Attenuation of the first 2 modes is worse than the single coating case in Fig. 4.3

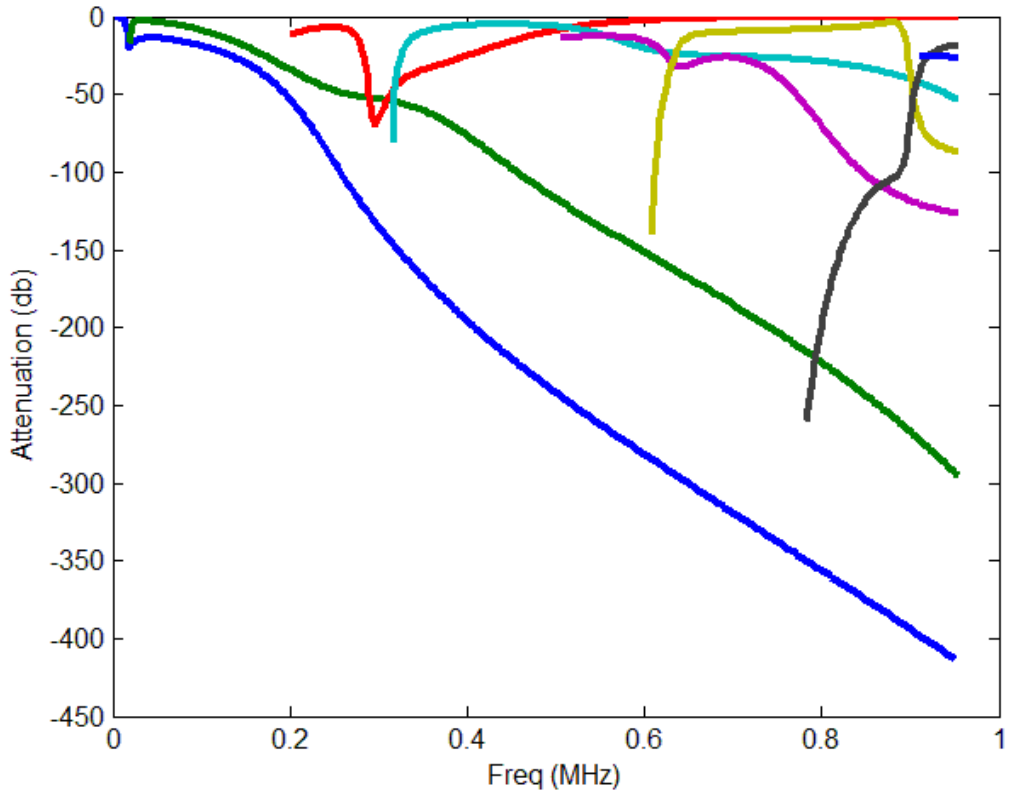

Fig. 4.5 attenuation dispersion curve of axial longitudinal wave of tubular with 2 epoxy layers

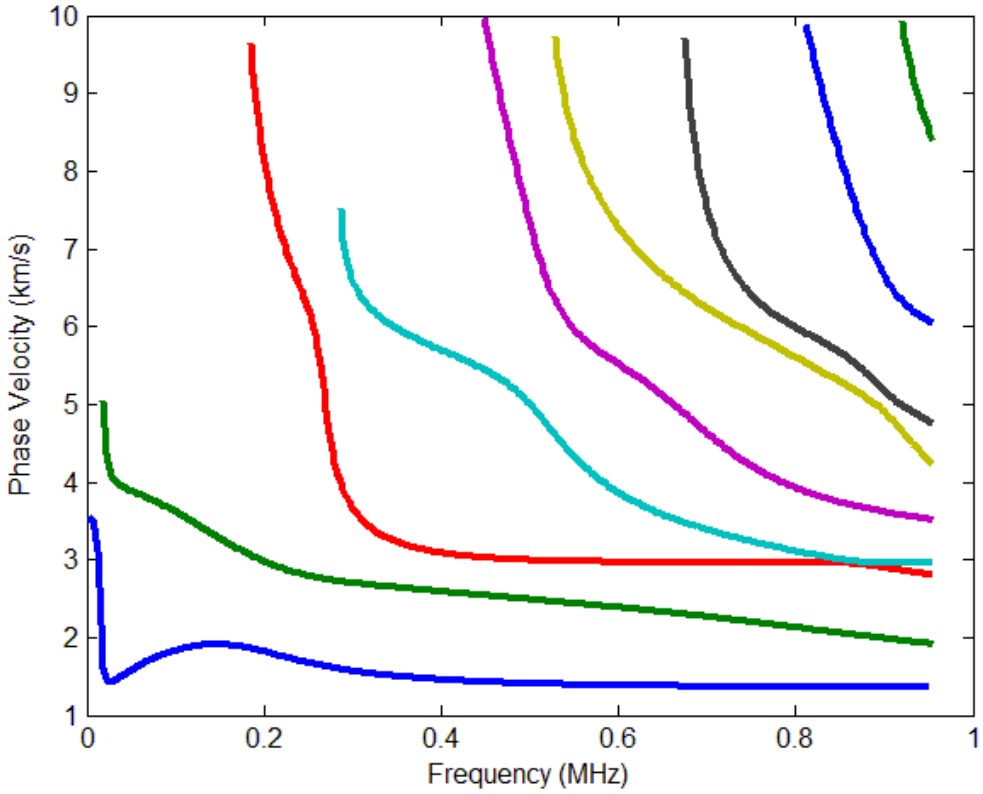

Fig. 4.6 Phase velocity dispersion curve of axial longitudinal wave in tubular with 3 epoxy layers

Observations made with Figs. 4.4 and 4.5 can be readily applied to Figs. 4.6 and 4.7. With the addition of one more epoxy layer, the wave dispersion is seen with one additional mode, and the differentiation of phase velocity at frequency higher than 1.0MHz among the highest seven modes is becoming even more difficult. Again, the 3rd mode suffers the least attenuation in the 0.4-0.8MHz frequency range.

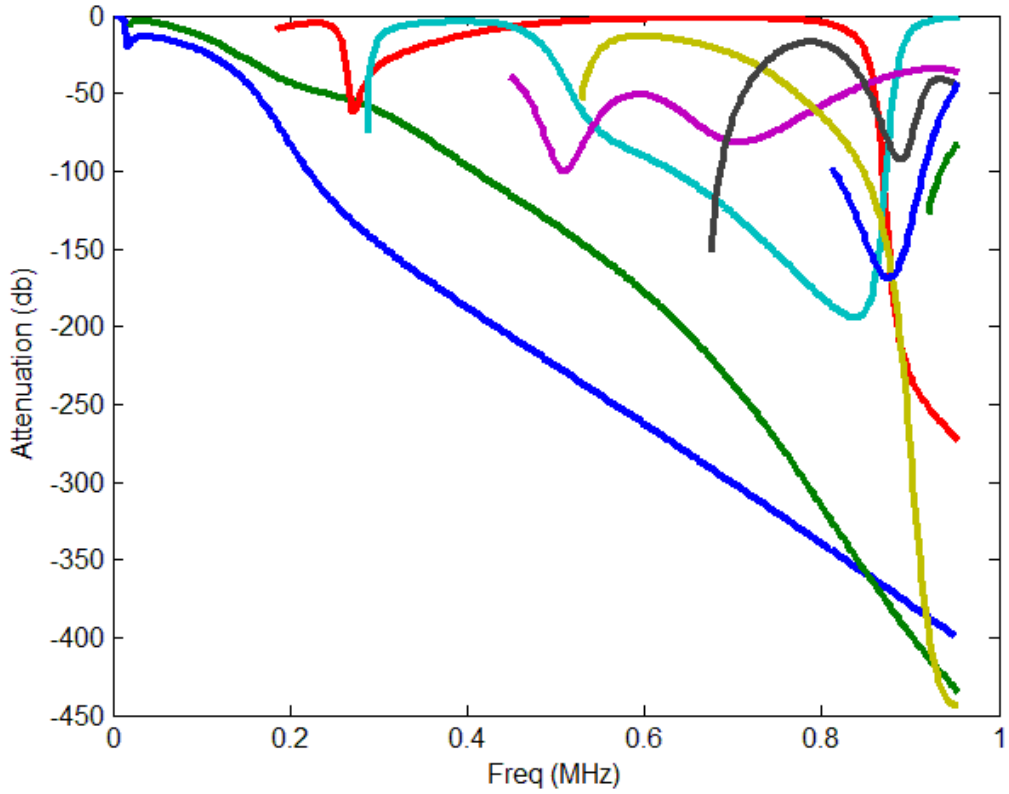

Fig. 4.7 Attenuation dispersion curve of axial longitudinal wave in tubular with 3 epoxy layers

4.3. Numerical Results of Shear Wave along Circumferential Direction

Using the same material properties and tubing parameters, the phase velocity dispersion of the shear wave propagated in a bare tubular section along the circumferential direction is considered in Fig. 4.8. There is only one mode at low frequency. More modes become admissible at higher frequency, and the resolution needed to differentiate them deteriorates as frequency increases.

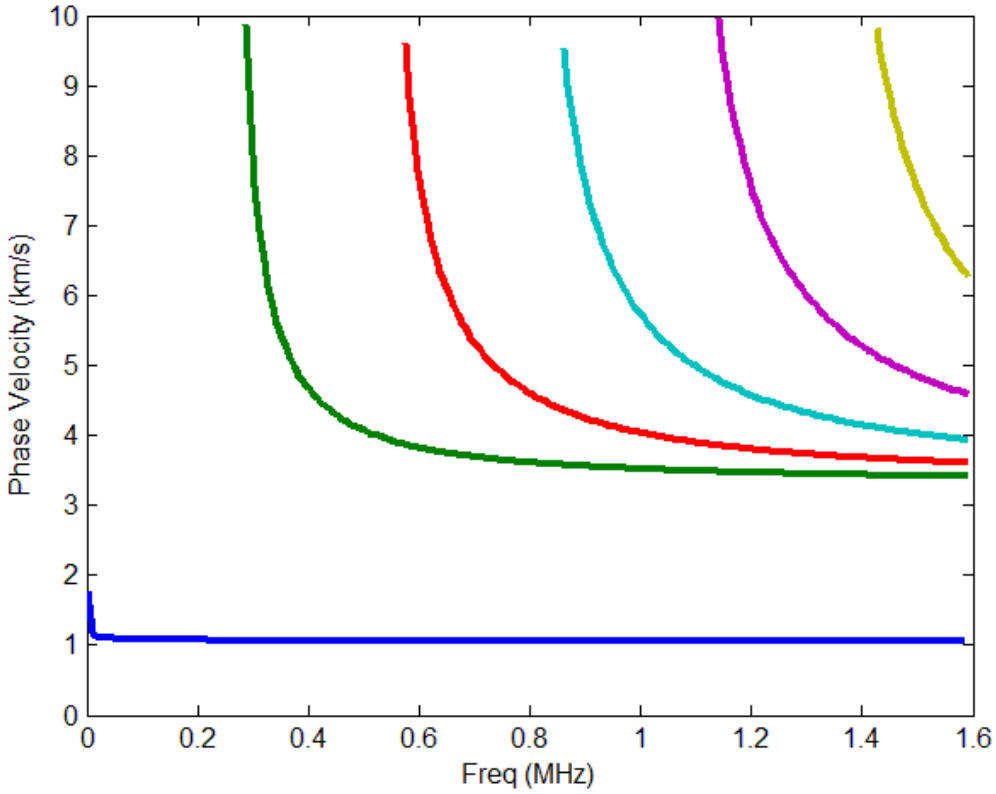

Fig. 4.8 Phase velocity dispersion curve of circumferential shear wave in bare tubing

The phase velocity and attenuation dispersion curves of the circumferential shear wave in the tubular with 1 layer of epoxy coating are shown in Figs. 4.9 and 4.10. Comparing the phase velocity dispersion for the single coating layer tubing to the baseline's (bare), several observations can be made: 1) there is an additional higher order mode; 2) the highest 5 modes rapidly converge to an asymptotic phase velocity at approximately 3.5km/sec; 3) the differentiation of the highest 5 modes at frequency higher than 1.6MHz becomes demanding; 4) the 1st mode has a cutoff frequency at about

0.52MHz; and 5) the 2nd mode demonstrates that it would fast attenuate. The attenuation dispersion curves in Fig. 4.10 further affirms observations 4) and 5) with the indications that the first 2 modes would soon dissipate upon initiation. Except for the 3rd mode which displays relatively low attenuation between 0.5-1.0MHz, all the higher order modes see significant attenuations at high frequency.

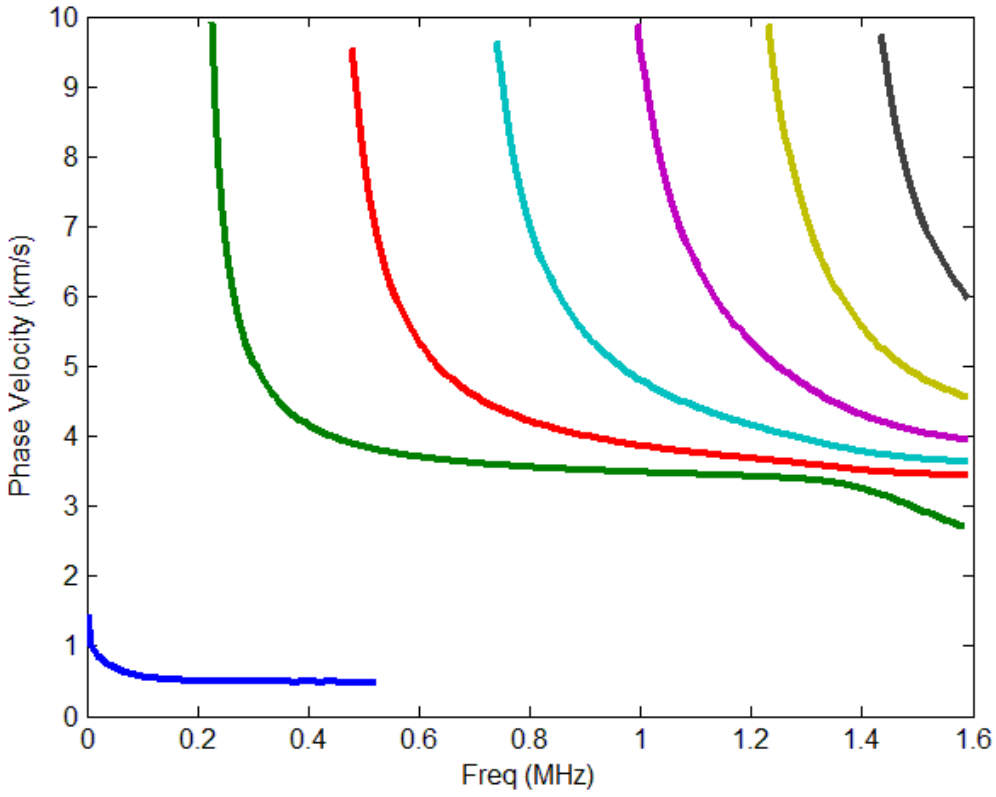

Fig. 4.9 Phase velocity dispersion curve of circumferential shear wave in tubular with 1 epoxy layer

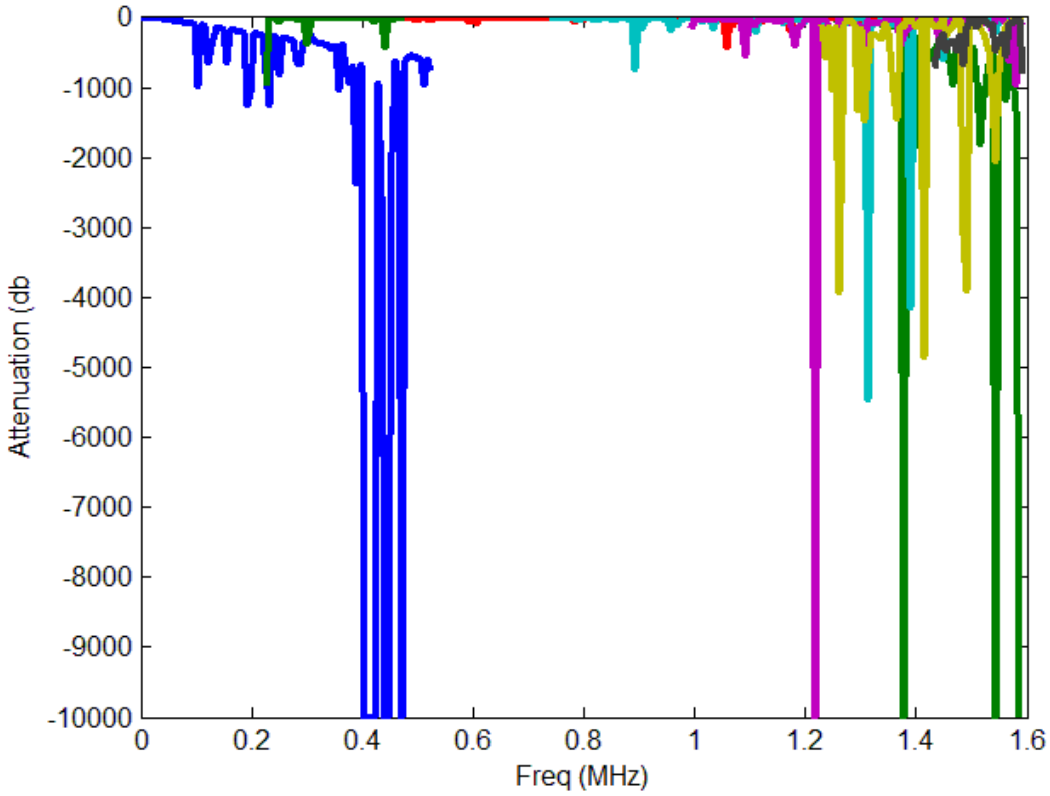

Fig. 4.10 Attenuation dispersion curve of circumferential shear wave in tubular with 1 epoxy layer

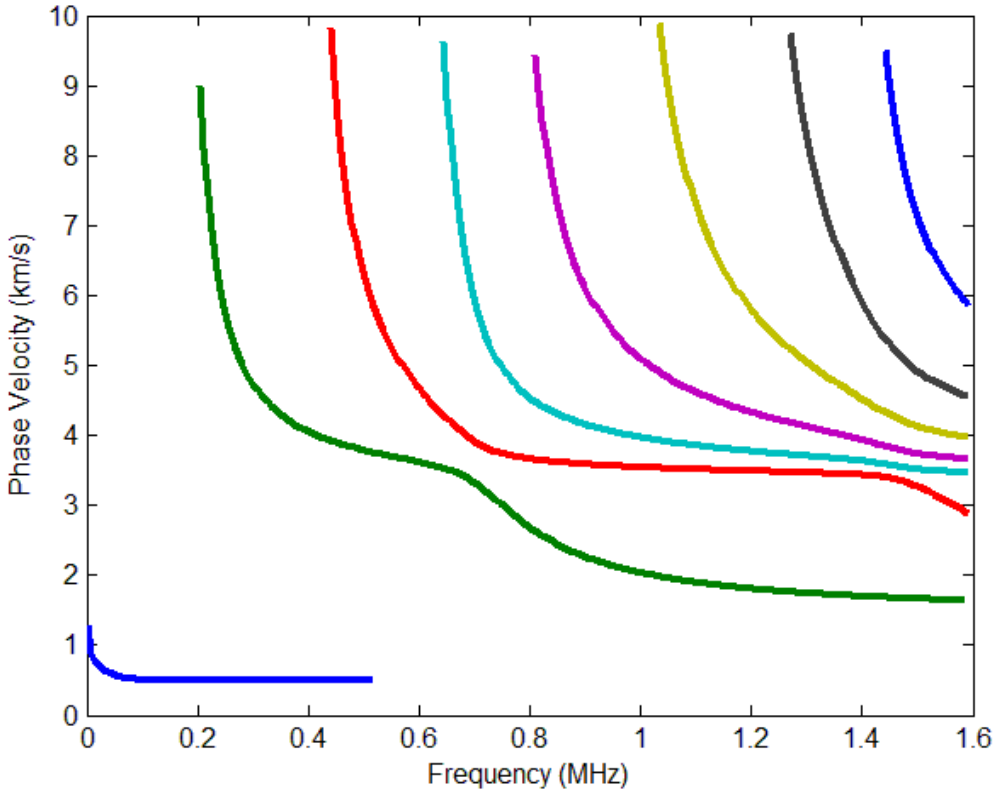

Fig. 4.11 Phase velocity dispersion curve of circumferential shear wave in tubular with 2 epoxy layers

Wave dispersion and attenuation of the circumferential shear wave correspond to 2 and 3 layers of viscoelastic coatings are plotted in Figs. 4.11-4.14. One additional mode is seen in Fig. 4.11 where the case of 2-layer coating is considered. The 4^{th}, 5^{th}, 6^{th}, and 7^{th} mode are seen fast approaching the non-dispersive asymptotic phase velocity with poor resolution in differentiating them at frequency higher than 1.6MHz. In addition to the 2^{nd} mode, the 3^{rd} mode is also fast dissipating. All admissible modes

suffer from significant attenuation, with the exception of the 2nd mode which demonstrates relatively low attenuation between 0.2 and 0.6MHz.

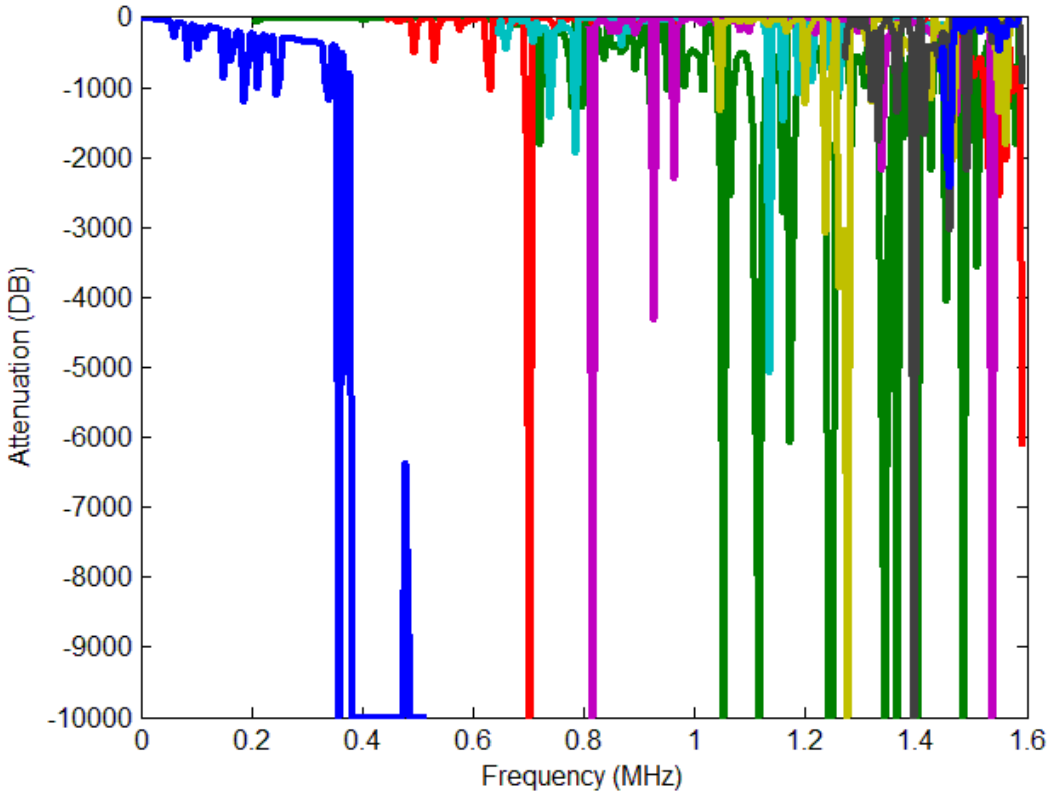

Fig. 4.12 Attenuation dispersion curve of circumferential shear wave in tubular with 2 epoxy layers

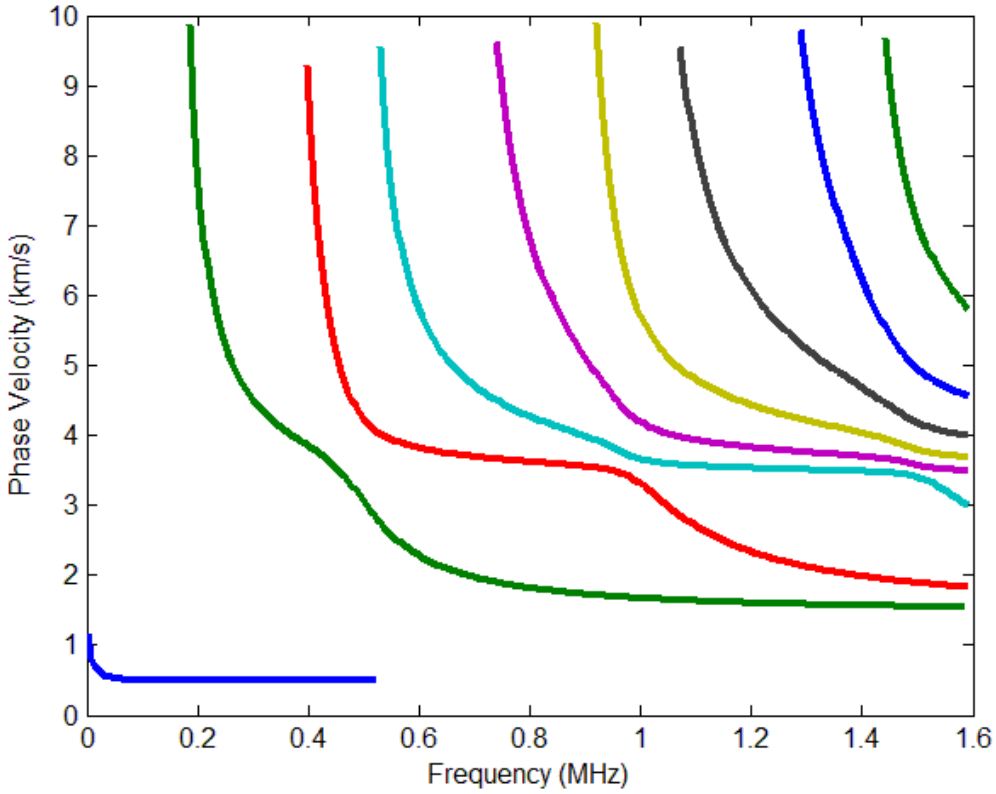

Fig. 4.13 Phase velocity dispersion curve of circumferential shear wave in tubular with 3 epoxy layers

Observations made for Figs. 4.11 and 4.12 can be readily applied to Figs. 4.13 and 4.14. With the addition of one more epoxy layer, the shear wave dispersion is seen with one additional mode in the 3 coated layers tubing model, and the differentiation of phase velocity at frequency higher than 1.6MHz among the highest four modes is becoming difficult. Now the 4th mode is also fast dissipating. Again, the 3rd mode suffers the least attenuation in the 0.4-0.8MHz frequency range. All admissible modes

suffer from significant attenuation, suggesting a probable physical scenario of short-lived propagation for all of them.

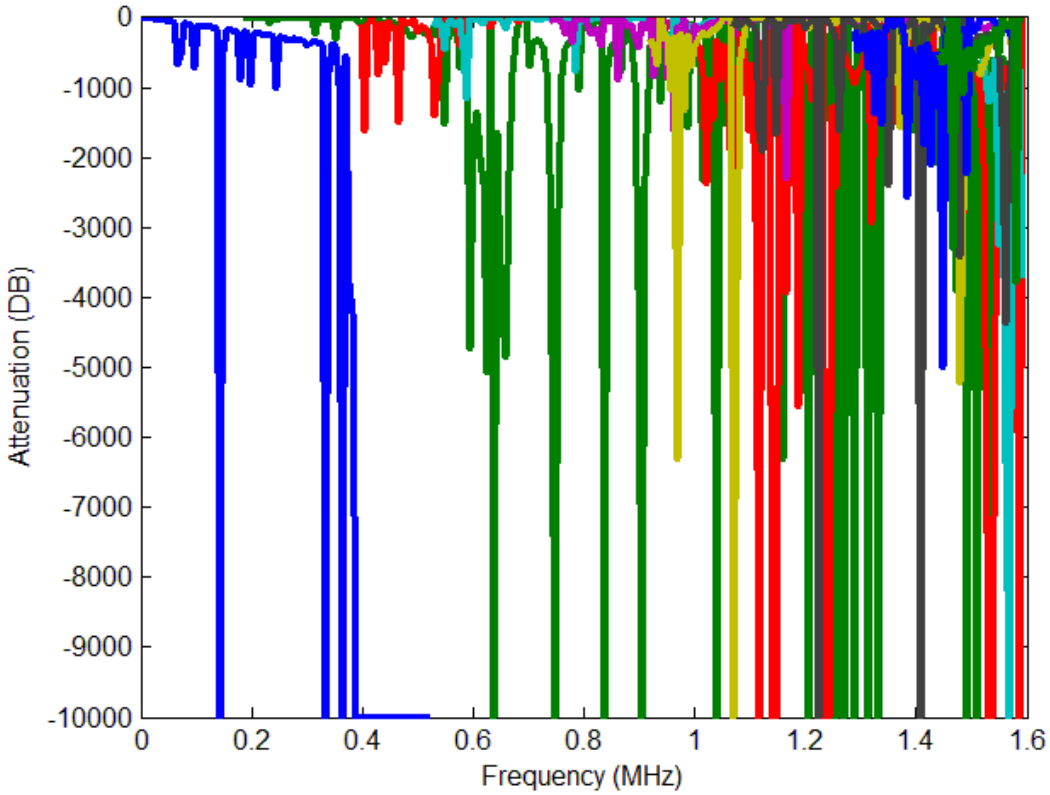

Fig. 4.14 Attenuation dispersion curve of circumferential shear wave in tubular with 3 epoxy layers

4.4. Numerical Results of Longitudinal Wave along Circumferential Direction

Using the same material properties and tubing parameters along with the numerical routine developed for finding real and complex roots, the phase velocity dispersion of the longitudinal wave propagated in a bare tubular section along the

circumferential direction is shown in Fig. 4.15. There are 2 modes at frequency 0-0.3MHz. More modes become admissible at higher frequency, and the various modes can be readily differentiated at a wide range of frequency with satisfactory resolution.

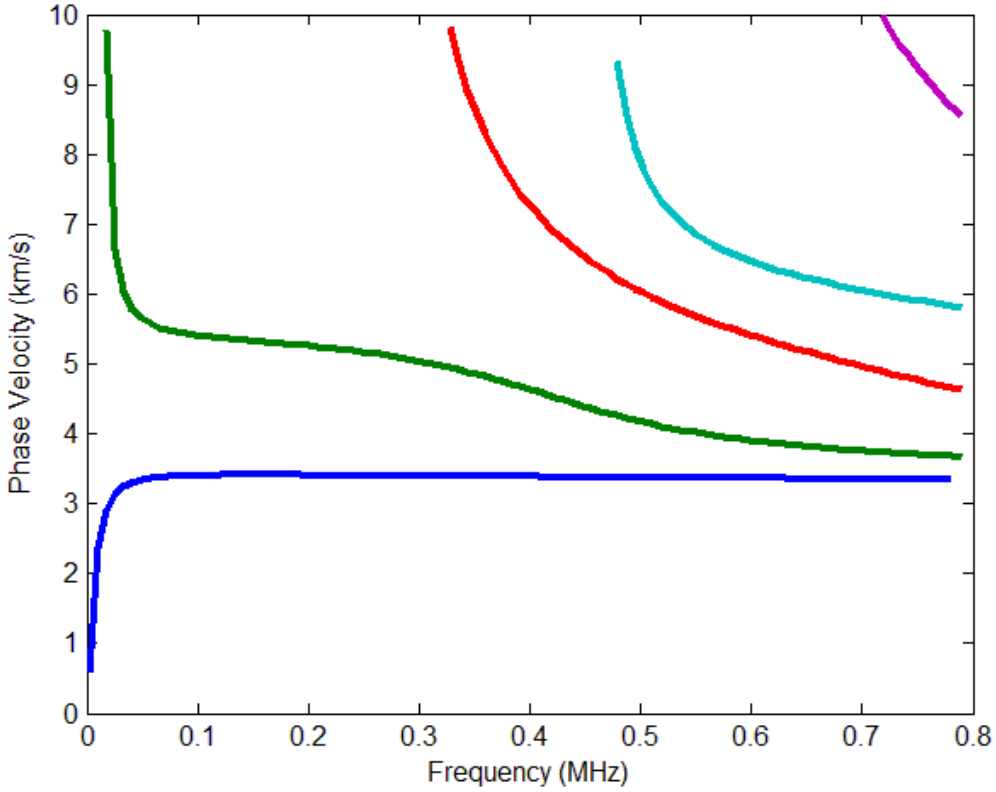

Fig. 4.15 Phase velocity dispersion curve of circumferential longitudinal wave in bare tubular

As oppose to Fig. 4.9, the 1st mode of the circumferential longitudinal wave in tubing coated with 1 layer of epoxy coating in Fig. 4.16 does not demonstrate a cutoff frequency. However, the mode along with the 2 mode does not converge to the non-

dispersive phase velocity but rather quickly dissipate with increasing frequency. This observation is also supported by the corresponding wave dispersion in Fig. 4.17 in which the 2nd mode is seen to be the only mode that displays low attenuation among all the admissible modes when the excitation/propagation frequency is lower than 0.18MHz. The most interesting feature in Fig. 4.16 is the overlapping of the two highest order modes. The two modes cannot be differentiated between the 0.71-0.74MHz frequency range. In addition, their corresponding high attenuations in Fig. 4.17 also suggest fast dissipation and, therefore, short life span.

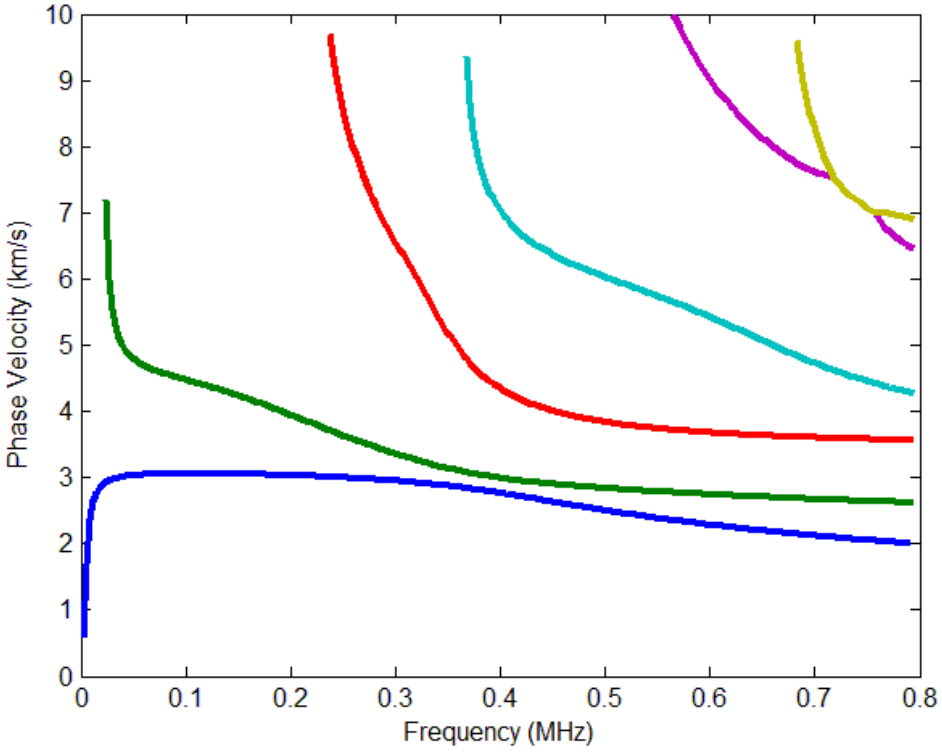

Fig. 4.16 Phase velocity dispersion curve of circumferential longitudinal wave in tubular with 1 epoxy layer

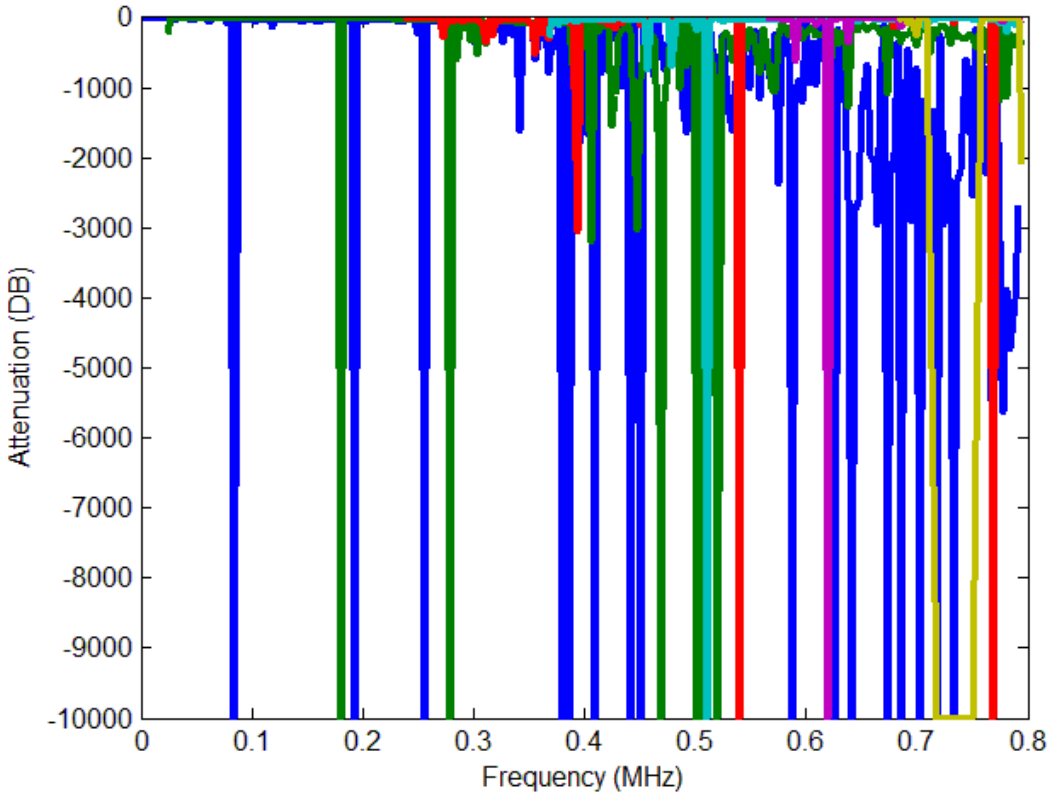

Fig. 4.17 Attenuation dispersion curve of circumferential longitudinal wave in tubular with 1 epoxy layer

Wave dispersion and attenuation of the circumferential longitudinal wave in tubing with 2 and 3 layers of viscoelastic coatings are plotted in Figs. 4.18-4.21. One additional mode is seen in Fig. 4.18 where the case of 2-layer coating is considered. The 3rd and 4th modes are fast approaching the non-dispersive asymptotic phase velocity with poor resolution in differentiating them at frequency higher than 0.8MHz. The dissipation of the first 2 modes is notably worse than the 1-layer case. All admissible

modes as seen in Fig. 4.19 suffer from significant attenuation, rendering the propagation of them all extremely brief and short-lived.

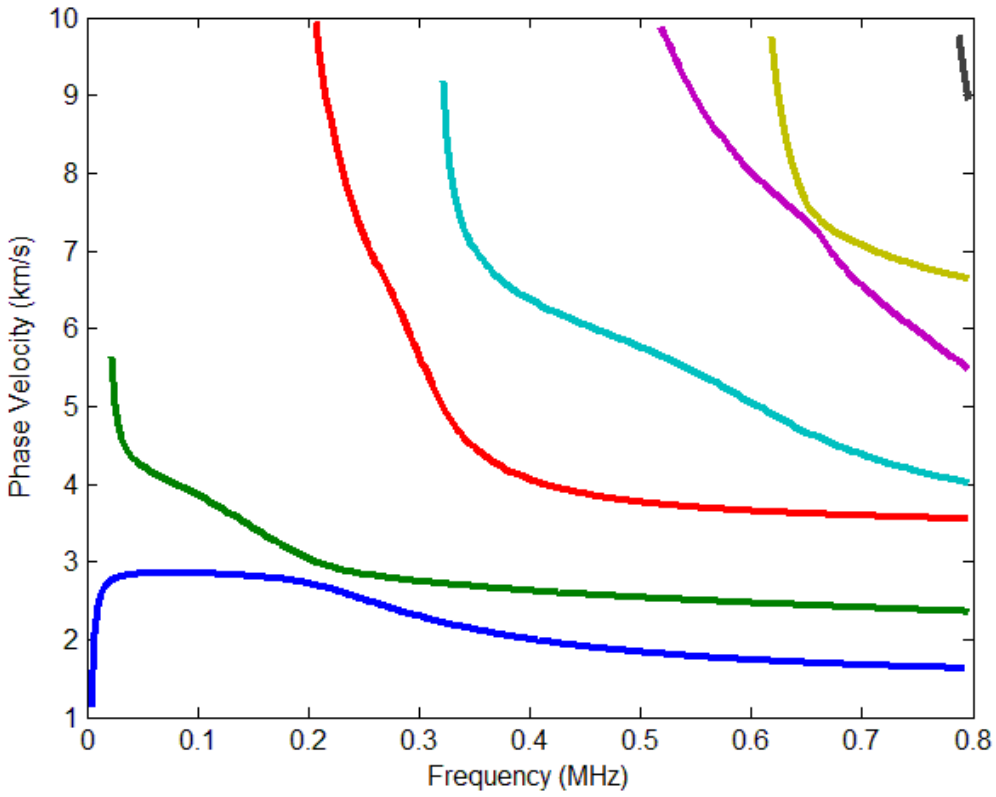

Fig. 4.18 Phase velocity dispersion curve of circumferential longitudinal wave in tubular with 2 epoxy layers

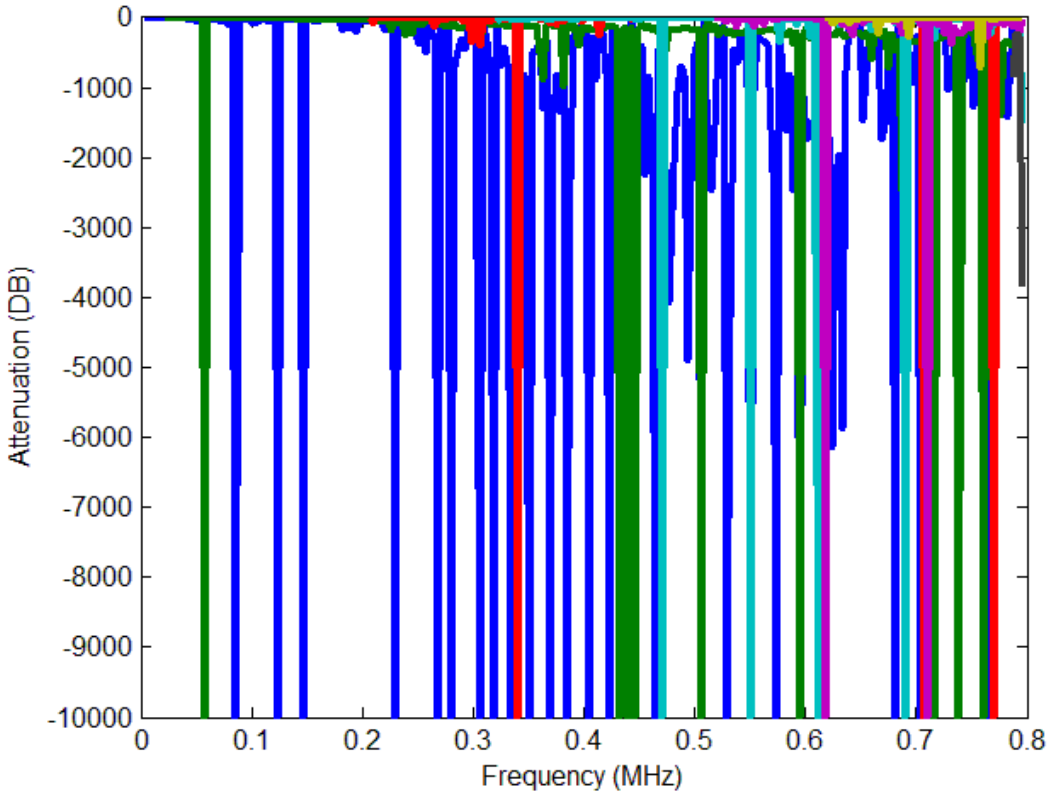

Fig. 4.19 Attenuation dispersion curve of circumferential longitudinal wave in tubular with 2 epoxy layers

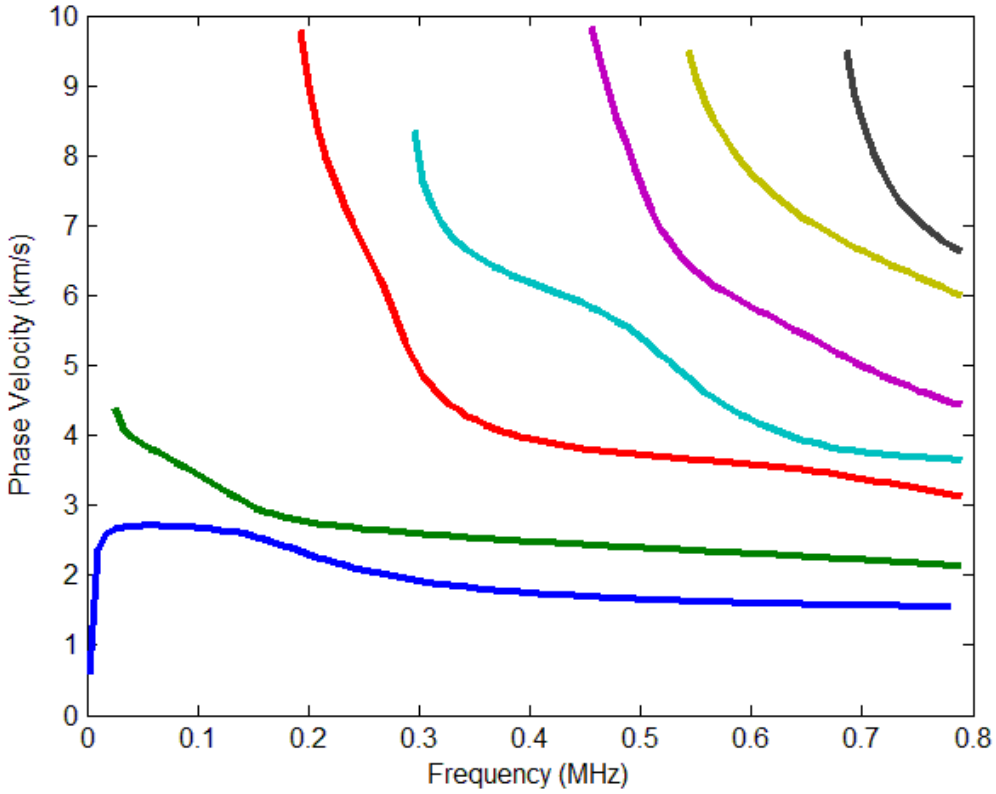

Fig. 4.20 Phase velocity dispersion curve of circumferential longitudinal wave in tubular with 3 epoxy layers

Observations made with Figs. 4.18 and 4.19 can be readily applied to Figs. 4.20 and 4.21. With the addition of one more epoxy layer, the circumferential longitudinal wave dispersion has one additional mode in the 3 coating layers tubing, and differentiating phase velocities at 0.8MHz or higher among the highest four modes becomes difficult. The 3rd mode is now also fast dissipating. Again, all admissible modes seen in Fig. 4.21 suffer from significant attenuation, a scenario substantially

worse than Fig. 4.19. This suggests that longitudinal wave propagation along the circumferential direction is not probable with the presence of 3 viscoelastic coatings.

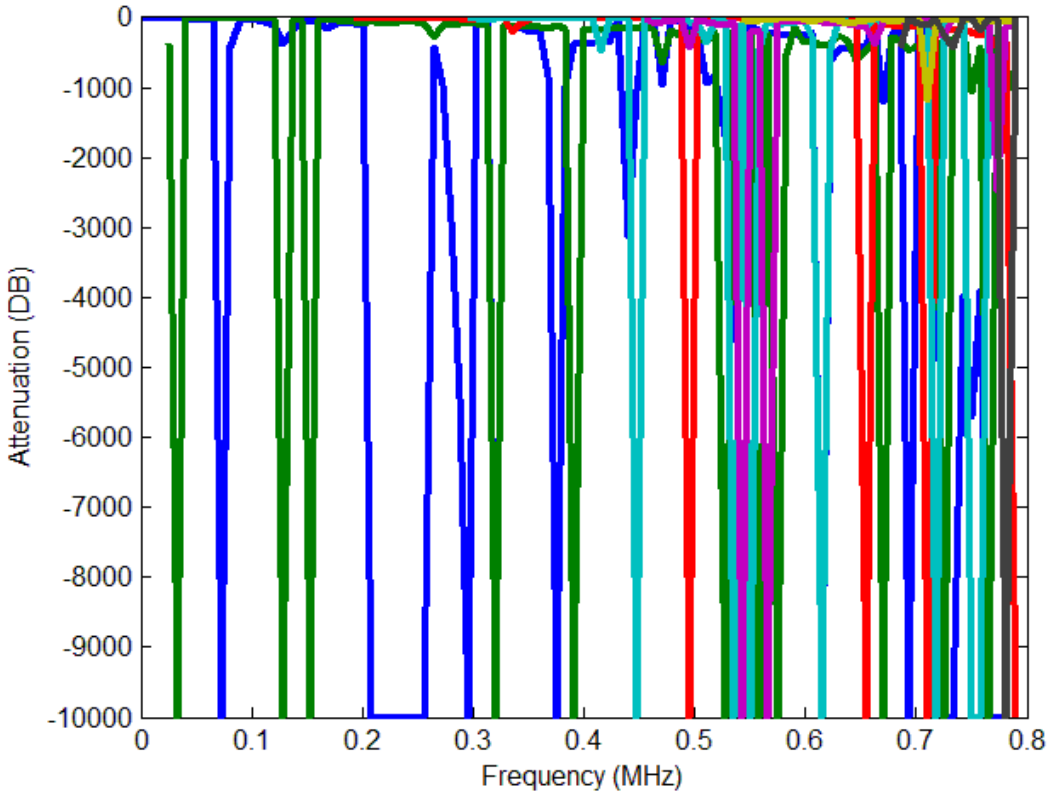

Fig. 4.21 Attenuation dispersion curve of circumferential longitudinal wave in tubular with 3 epoxy layers

4.5. Discussions

It was seen that in general the wider the frequency window considered the more modes were admissible. The number of admissible modes also increased with increasing number of viscoelastic coating layers. It was also observed using all the attenuation dispersion curves that attenuation became large at the frequency where the corresponding phase velocity precipitated. As the coating number increased, wave motions along both the axial and circumferential directions were characterized by substantial attenuation and effectively suppressed. The study showed that no mode could be propagated in steel tubing coated with more than 3 layers of epoxy coating.

From the practical point of view, it is essential to identify the proper mode that is the least attenuative at certain frequency range. In order to better understand the nature of attenuation dispersion, the effect of increasing α value is examined. Figs. 4.22 and 4.23 show the results correspond to increasing α by 20% from its original value for the case of axial longitudinal wave in tubing coated with 1 layer of epoxy.

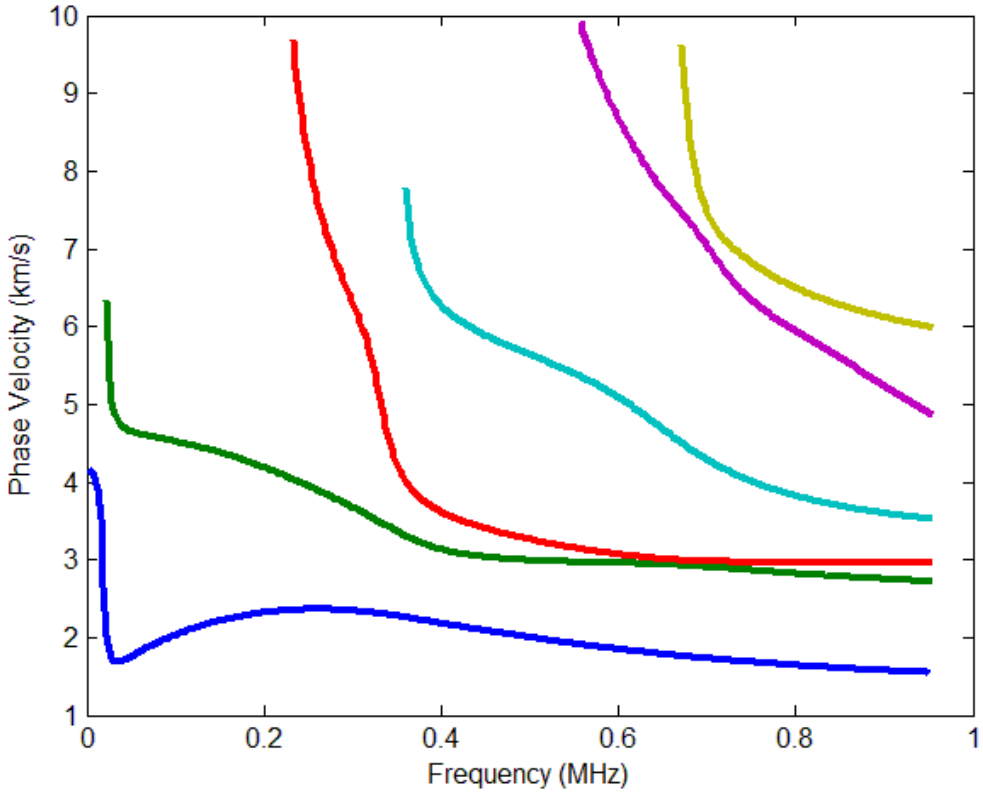

Fig. 4.22 Phase velocity dispersion curve of axial longitudinal wave in tubular with 1 epoxy layer coating with α being increased by 20%

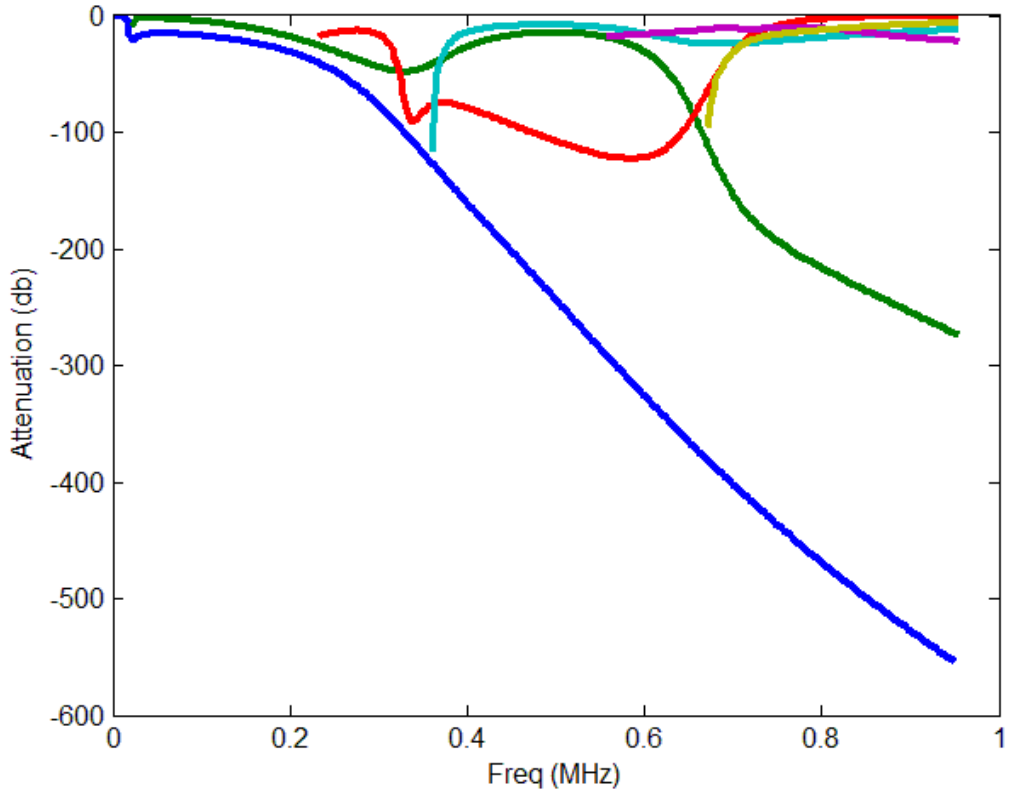

Fig. 4.23 Attenuation Dispersion Curve of Axial Longitudinal Wave of Tubular with 1 Layer Epoxy Coating which Increased α 20%

Comparing Fig. 4.22 with Fig. 4.2, it is evident that the greater α value does not impose an effect on the phase velocity dispersion. However, all the modes in the corresponding attenuation dispersion in Fig. 4.23 are seen to increase in attenuation magnitude. The proper interpretation of these results would be that once a particular mode is excited at a specific frequency, it is the attenuation of the coating material that dictates the propagation and termination of the mode.

Next is to examine the effect of increasing coating thickness. The thickness is increased by 20% from its original value.

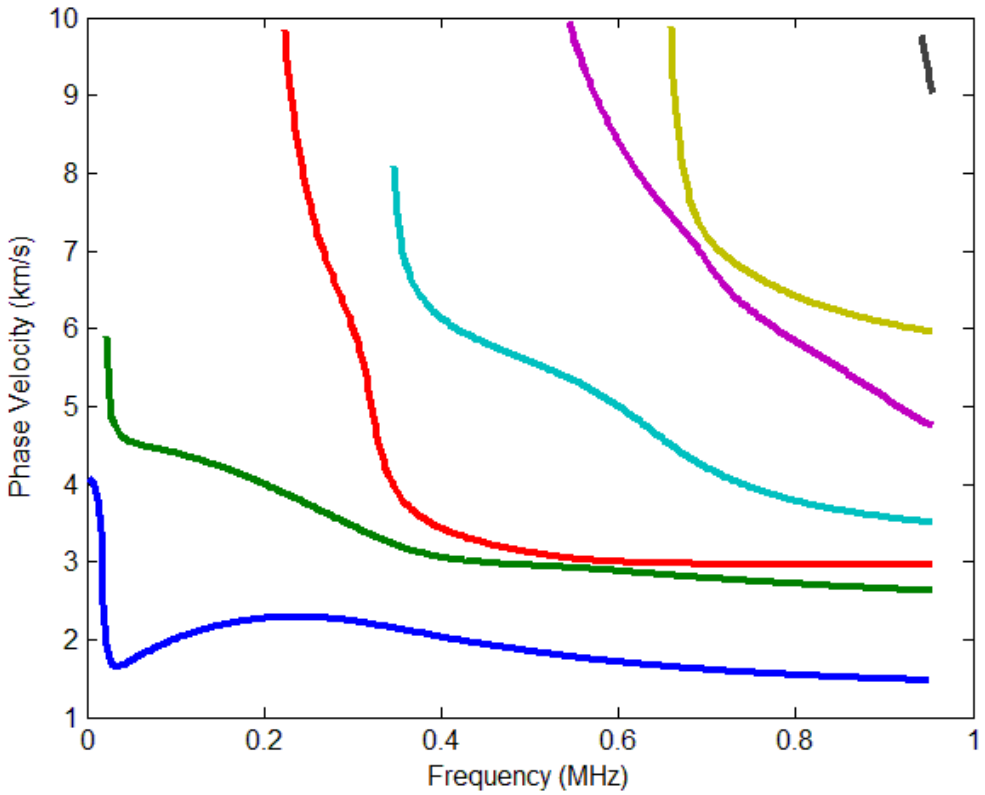

Fig. 4.24 Phase velocity dispersion curve of axial longitudinal wave in tubular with 1 epoxy layer coating with coating thickness being increased 20%

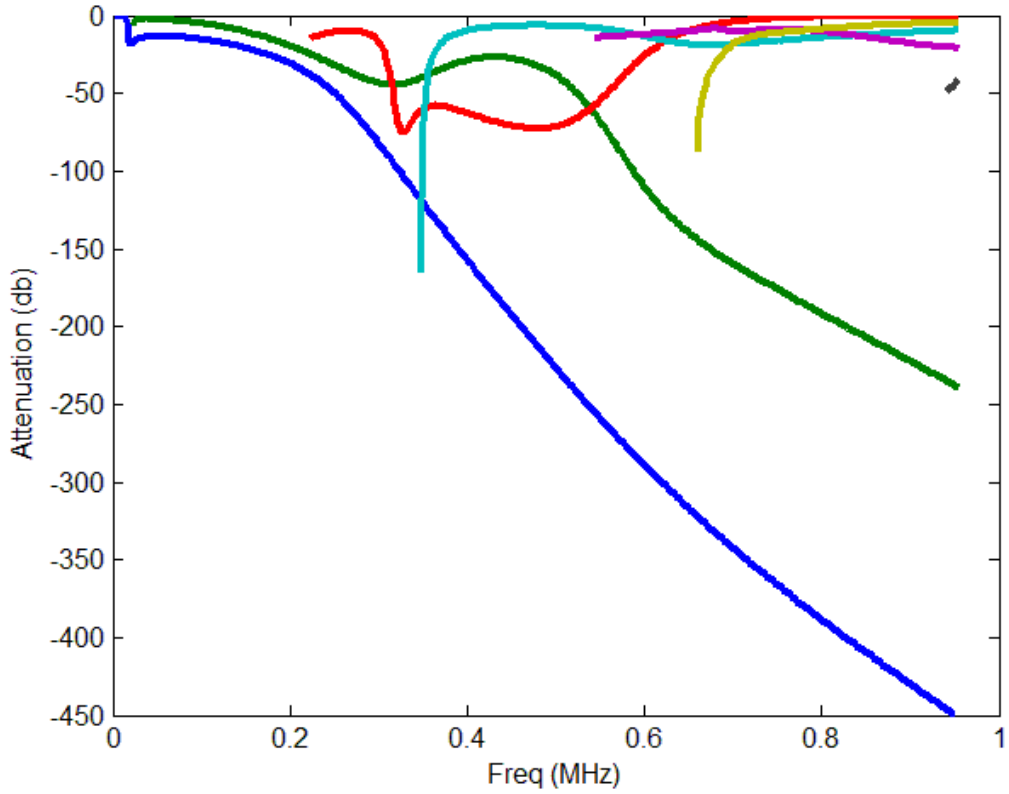

Fig. 4.25 Attenuation dispersion curve of axial longitudinal wave in tubular with 1 epoxy layer coating with coating thickness being increased 20%

Comparing Figs. 4.24 and 4.25 with Figs. 4.2 and 4.3, it is seen that the phase velocity dispersion is affected by having an additional higher order mode – a scenario comparable to adding another coating layer characteristically similar to Fig. 4.4 where a 2-layer epoxy coating was considered. While the phase velocity dispersion is visibly affected, however, the attenuation dispersion is not. Therefore, it is concluded that the selection of viscoelastic coating materials and the application of them as protective layers to tubular have a substantial impact on the propagation and attenuation of various

wave modes. The implications are broad and significant in engineering applications in that improper choice of coating materials could result in high cost, low efficiency, and poor resolution.

5. SUMMARY AND FUTURE WORK

5.1. Summary

In Sec. 2 the Navier's governing equation of motion for a tubular section was derived in the cylindrical coordinates. Longitudinal wave motions in the axial direction and shear and longitudinal wave motions in the circumferential direction were considered. After the layer matrices for each of the propagation mode were developed, proper boundary conditions corresponding to perfectly bonded layers were then applied. The condition imposed was the continuity of displacement and strain between the interfacial layers and stress-free for the exposed layers. The global matrices of each of the model were first assembled with the imposed boundary conditions for a coated hollow pipe with multiple elastic layers.

In Sec. 3 the general stress-strain relationship for viscoelastic materials was described in which the correspondence principle was applied to show how viscoelastic material properties can be incorporated into the constitutive law to model the propagation of harmonic waves in epoxy-coated pipes. The bisection numerical routine for finding both the real and complex roots of the three characteristic dispersion equations was also introduced. In particular the wave dispersion solution of the bare elastic tubing was employed as the initial guess for finding the complex roots for the system of equations of the viscoelastically-coated tubing. It was assumed that the complex wavenumbers of the viscoelastic solutions had their real parts close to the real wavenumbers associated with the elastic solutions.

Phase velocity and attenuation corresponding to each mode of propagation were established as functions of frequency in Sec. 4. The dispersion of phase velocity and wave attenuation for coated pipes were evaluated against a baseline model which was the bare, uncoated tube to establish the propagation characteristics of guided shear and longitudinal waves in the presence of multiple coating layers. It was observed that 1) the number of modes increases with increasing number of viscoelastic layers, 2) while more admissible modes can be excited; however, the resolution in phase velocity in terms of differentiating them becomes poor, 3) the first few lower order modes all suffer from significant attenuation, thus rendering the employment of them not feasible for practical purpose, and 4) higher order modes would attenuate almost negligibly at high frequencies. In the last part of the presentation, the effects of increasing attenuation parameter α and coating thickness were investigated. It was found that the attenuation dispersion curves were highly sensitive to the parameter α but relatively insensitive to the coating thickness. In other words, the larger the attenuation parameter, the more effective the viscoelastic coated layers in dissipating the wave energy. Both the phase velocity dispersion and attenuation curves were sensitive to increasing coating thickness. However, the effect of thickness on wave attenuation was considered secondary as it was not as prominent as the attenuation parameter α.

5.2. Future Work

The research has generated in-depth understanding of the fundamental propagation characteristics of three types of guided waves in the elastic tubing coated

with layers of thin viscoelastic materials. The derivation and modeling presented in the thesis are expected to have significant implications in employing the circumferential shear and longitudinal waves for characterizing coated pipe. In addition, the presented results on wave dispersion and attenuation would help develop a viable ultrasonic technology that is of high time and frequency resolutions and optimal in resolving mechanical defects and coating flaws simultaneously.

As a theoretical endeavor, the thesis is comprehensive and complete. However, efforts are still needed to promote its applicability and to realize broader impact. The first would be to validate the theory along with the guided wave models through performing physical testing. A carefully developed experimental test plan with proper instrumentation would be required. The second would be to optimize the root-search algorithm to allow more modes of higher orders at still higher frequencies to be explored with improved computational efficiency.

REFERENCES

[1] Gazis, D. C., 1959, "Three-Dimensional Investigation of the Propagation of Waves in Hollow Circular Cylinders. I. Analytical Foundation," The Journal of the Acoustical Society of America, **31**(5), pp. 568-573.

[2] Gazis, D. C., 1959, "Three-Dimensional Investigation of the Propagation of Waves in Hollow Circular Cylinders. II. Numerical Results," The Journal of the Acoustical Society of America, **31**(5), pp. 573-578.

[3] Liu, G., and J. Qu, 1998, "Guided Circumferential Waves in a Circular Annulus," Journal of Applied Mechanics, **65**(2), pp. 424-430.

[4] Valle, C., Niethammer, M., Qu, J., and Jacobs, L., 2001, “Crack Characterization Using Guided Circumferential Waves,” Journal of the Acoustical Society of America, **110**, pp. 1282–1290.

[5] Hirao, M., and Ogi, H., 1999, “An SH-wave EMAT Technique for Gas Pipeline Inspection,” NDT & E International, **32**(3), pp. 127-132.

[6] Gao, W., Glorieux, C., and Thoen, J., 2002, “Study of Circumferential Waves and Their Interaction with Defects on Cylindrical Shells Using Lline-Source Laser Ultrasonics,” Journal of Applied Physics, **91**(9), pp. 6114-6119.

[7] Baltazar-López, M., Burger, C., Chona, R., and Suh, S., 2005, “Study of Wave Motion on Tubulars Using Broad-Band Laser Ultrasound,” Experimental Mechanics, **45**(5), pp. 427-432.

[8] Niethammer, M., Jacobs, L. J., Qu, J., and Jarzynski, J., 2001, “Time-Frequency Representations of Lamb Waves,” The Journal of the Acoustical Society of America, **109**(5), pp. 1841-1847.

[9] Liew, K. M., and Wang, Q., 1998, “Application of Wavelet Theory for Crack Identification in Structures,” Journal of Engineering Mechanics, **124**(2), pp. 152-157.

[10] Kim, H., and Melhem, H., 2003, “Fourier and Wavelet Analyses for Fatigue Assessment of Concrete Beams,” Experimental Mechanics, **43**(2), pp. 131-140.

[11] Kley, M., Valle, C., Jacobs, L. J., Qu, J., and Jarzynski, J., 1999, “Development of Dispersion Curves for Two-Layered Cylinders Using Laser Ultrasonics,” The Journal of the Acoustical Society of America, **106**(2), pp. 582-588.

[12] Valle, C., Qu, J., and Jacobs, L. J., 1999, “Guided Circumferential Waves in Layered Cylinders,” International Journal of Engineering Science, **37**(11), pp. 1369-1387.

[13] Jones, J. P., 1964, ‘‘Wave Propagation in a Two-Layered Medium,’’ Journal of Applied Mechanics, **31**, pp. 213–222.

[14] Laperre, J., and Thys, W., 1993, “Experimental and Theoretical Study of Lamb Wave Dispersion in Aluminum/Polymer Bilayers,” The Journal of the Acoustical Society of America, **94**(1), pp. 268-278.

[15] Simonetti, F., 2004, “Lamb Wave Propagation in Elastic Plates Coated with Viscoelastic Materials,” The Journal of the Acoustical Society of America, **115**(5), pp. 2041-2053.

[16] Zhu, Z., and Wu, J., 1995, "The Propagation of Lamb Waves in a Plate Bordered with a Viscous Liquid," The Journal of the Acoustical Society of America, **98**(2), pp. 1057-1064.

[17] Nayfeh, A. H., and Nagy, P. B., 1997, “Excess Attenuation of Leaky Lamb Waves Due to Viscous Fluid Loading,” The Journal of the Acoustical Society of America, **101**(5), pp. 2649-2658.

[18] Luo, W., Rose, J. L., Velsor, J. K. V., Avioli, M., and Spanner, J., 2006, “Circumferential Guided Waves for Defect Detection in Coated Pipe,” *AIP Conference Proceedings,* Brunswick, Maine, **820**(1), pp. 165-172.

[19] Barshinger, J. N., and Rose, J. L., 2004, “Guided Wave Propagation in an Elastic Hollow Cylinder Coated with a Viscoelastic Material,” Ultrasonics, Ferroelectrics and Frequency Control, IEEE Transactions on, **51**(11), pp. 1547-1556.

[20] Knopoff, L., 1964, “A Matrix Method for Elastic Wave Problems,” Bulletin of the Seismological Society of America, **54**(1), pp. 431-438.

[21] Lowe, M.J.S., 1995, “Matrix Techniques for Modeling Ultrasonic Waves in Multilayered Media”, IEEE Transactions on Ultrasonics, Ferroelectrics and Frequency Control, **42**(4), pp. 525-542.

[22] BME456: Constitutive Equations: Viscoelasticity, n.d., from http://www.engin.umich.edu/class/bme456/ch7consteqviscoelasticity/bme456consteqviscoelasticity.htm

[23] Christensen, R. M., 1981, *Theory of Viscoelasticcity: An Introduction*, Academic, New York.

[24] Schwab, F., 1970, “Surface Wave Dispersion Computations: Knopoff's method,” Bulletin of the Seismological Society of America, **60**(5), pp. 1491-1520.

[25] Carbon, Alloy and Stainless Steel Pipes - ASME/ANSI B36.10/19, n.d., from http://www.engineeringtoolbox.com/steel-pipes-dimensions-d_43.html

[26] Luo, W., and Rose, J. L., 2007, “Phased Array Focusing With Guided Waves in a Viscoelastic Coated Hollow Cylinder,” The Journal of the Acoustical Society of America, **121**(4), pp. 1945-1955.

[27] Blanc, R.H., 1993, “Transient Wave Propagation Methods for Determining the Viscoelastic Properties of Solids,” Journal of Applied Mechanics, **60**(3), pp. 763-768.